Weak coupling of fluvial aggradation and paleo-denudation rates during the last glacial cycle, Crete, Greece

Richard F. Ott[1], Dirk Scherler[1,2], Karl W. Wegmann[3], Mitch K. D'Arcy[4], Richard J. Pope[5], Susan Ivy-Ochs[6], Marcus Christl[6], Christoph Vockenhuber[6], Tammy M. Rittenour[7]

[1]GFZ German Centre for Geoscience Research, Potsdam, Germany

[2]Institute of Geological Sciences, Freie Universität Berlin, Berlin, Germany

[3]Department of Marine, Earth and Atmospheric Sciences & Center for Geospatial Analytics, North Carolina State University, Raleigh, NC, U.S.A.

[4]Department of Earth, Ocean and Atmospheric Sciences, University of British Colombia, Vancouver, Canada

[5]School of Environmental Sciences, College of Built and Natural Environment, University of Derby, Derby, United Kingdom

[6]Laboratory of Ion Beam Physics, ETH Zurich, Zurich, Switzerland

[7]Geosciences Department, Utah State University, U.S.A.

Corresponding author: Richard Ott (richard.ott@gfz-potsdam.de). Telegrafenberg, 14473 Potsdam, Germany

This is a non-peer reviewed preprint. This manuscript has been submitted to Earth Surface Processes and Landforms. If accepted, the final version of this manuscript will be available via the 'Peer-reviewed Publication DOI' link on the right hand side of this webpage.

Abstract

The impact of Quaternary climate cycles on denudation rates and fluvial aggradation and incision is debated, especially in non-glaciated regions. Here we present paleo-denudation rates and geochronological constraints on aggradation and incision from the Sfakia and Elafonisi alluvial-fan sequences on Crete, Greece. We report seven optically stimulated luminescence (OSL), ten radiocarbon ages, and eight ^{10}Be and eight ^{36}Cl denudation rates from modern and terrace sediments. For five samples, ^{10}Be and ^{36}Cl were measured on the same sample by measuring ^{10}Be on cherts and ^{36}Cl on calcite. Results indicate relatively steady denudation rates throughout the past 80kyr, but the aggradation and incision history indicate a link with shifts in climate. At the Elafonisi fan, we identify four periods of aggradation coinciding with Marine Isotope Stages (MIS) 2, 4, 5a/b, and likely 6, and three periods of incision coinciding with MIS 1, 3, and likely 5e. At the Sfakia fan, rapid aggradation occurred during MIS 2 and 4, analogous to aggradation periods at the Elafonisi fan system, followed by up to 50 m of incision during MIS 1. Nearby climate and vegetation records show that MIS 2, 4, and 6 were characterized by cold and dry climates with sparse vegetation, whereas forest cover and wet conditions prevailed during MIS 1, 3, and 5. Our data thus suggest that past changes in climate had little effect on landscape-wide denudation rates, but exerted a strong control on the aggradation-incision behaviour of alluvial channels on Crete. During glacial stages, we attribute aggradation to hillslope sediment release promoted by reduced vegetation cover and decreased river sediment transport capacity; conversely, incision occurred during relatively warm and wet stages due to increased river transport capacity. We conclude that, in this landscape, past hydroclimate variations outcompeted changes in sediment supply as the primary driver of alluvial deposition and incision.

Keywords: denudation, erosion, glacial, aggradation, incision, cosmogenic nuclides, luminescence

1 Introduction

The impact of Quaternary glacial cycles on denudation rates has long been debated. Several studies have suggested that a shift to a glacial climate intensifies physical erosion processes such as frost-cracking and therefore increases denudation rates at a local (e.g., Shuster et al., 2005; Vernon et al., 2008; Berger et al., 2008; Valla et al., 2012) and even global scale (Peizhen et al., 2001; Herman et al., 2013). Other studies have argued that inferences from thermochronologic and sedimentary records are biased and that erosion was steady throughout the late Cenozoic cooling period (Willenbring and von Blanckenburg, 2010; Willenbring and Jerolmack, 2016) or that evidence for an increase remains ambiguous (Schildgen et al., 2018). However, the denudation response to climate change may vary locally depending on the major denudation processes, causing non-glaciated areas to respond differently to glaciated regions, even if nearby (Mariotti et al., 2021). In addition to denudation, Quaternary glacial cycles may influence sediment production, transport, and deposition, by changing the transport capacity of streams and the amount of sediment supplied to them (Bull, 1991). Such differences in geomorphic response to Quaternary glacial cycles are known to vary in between climate zones (Richardson et al., 2019). Therefore, studying alluvial responses to climate change in different settings is imperative to understand the impact of climate change on landscapes.

Paleo-denudation rates from cosmogenic nuclides are a useful tool for quantifying denudation throughout the Quaternary (e.g., Kapannusch et al., 2020; Lenard et al., 2020; Mariotti et al., 2021). Cosmogenic nuclide concentrations measured in alluvial sediments can be used to calculate paleo-denudation rates, provided that concentrations can be corrected for nuclide production and decay after sediment deposition (Schaller et al., 2002). These paleo-denudation rates can then be compared with past climate (Mason and Romans, 2018) and aggradation-incision records (Scherler et al., 2015) to study the geomorphic response to climate change. Such aggradation-incision records are sensitive to fluxes in hillslope-to-channel sediment delivery and water discharge, which controls the stream transport capacity (Bull, 1991). Several studies have used this behaviour to demonstrate that aggradation of alluvial and submarine fans record variations in catchment sediment export in response to Quaternary climate cycles (Pope and Wilkinson, 2005; Waters et al., 2010; D'Arcy et al., 2017a; Watkins et al., 2019).

Despite the growing number of paleo-denudation studies, it remains unclear if denudation in temperate fluvial landscapes increased during a colder climate due to enhanced physical erosion (Hales and Roering, 2007; Marshall et al., 2021). In temperate climates, Marshall et al. (2015) showed a 2.5-fold increase in denudation during glacial conditions using cosmogenic nuclides whereas other studies could not detect any significant variations in denudation in Pleistocene deposits (Schaller et al., 2002; Cyr and Granger, 2008; Kapannusch et al., 2020). In the southwestern US, Pleistocene paleo-denudation rates show only minor variations across orbitally-driven hydroclimate cycles (Mason and Romans, 2018). Yet, it has been argued that alluvial fans record major concurrent variations in catchment sediment flux (D'Arcy et al., 2017b) and potentially in storm rainfall intensity in the case of debris-flow fans (D'Arcy et al., 2017a). Because such alluvial records respond to changes in hillslope sediment delivery and sediment transport

capacity, few studies have disentangled whether aggradation-incision is driven by changes in sediment flux, water discharge, or both (Wegmann and Pazzaglia, 2009). As short source-to-sink systems, alluvial fans respond rapidly to changing climatic conditions. When coupled with paleo-denudation rate measurements, alluvial fans are ideal for investigating how climate changes affect hillslope sediment supply to channels and how such variations in supply are transferred into the sedimentary record.

To investigate the response of hillslope denudation and stream aggradation-incision behaviour to climate variations in a fluvial landscape, we studied Late Pleistocene deposits of the Sfakia and Elafonisi fan complexes in western Crete, Greece (Fig. 1). We take advantage of geochronologic ages published for the Sfakia fan (Pope et al., 2008, 2016) and contribute new geomorphic mapping results, luminescence, and radiocarbon dating for the Elafonisi fan system. In addition, to studying changes in hillslope denudation, we measured cosmogenic ^{10}Be and ^{36}Cl in quartz-bearing and limestone lithologies, respectively, from modern and Late Pleistocene sediment. Together, these data allow us to compare variations in aggradation and incision with concurrent hillslope denudation rates and investigate the sensitivity of the sedimentary record to variations in transport capacity and sediment supply.

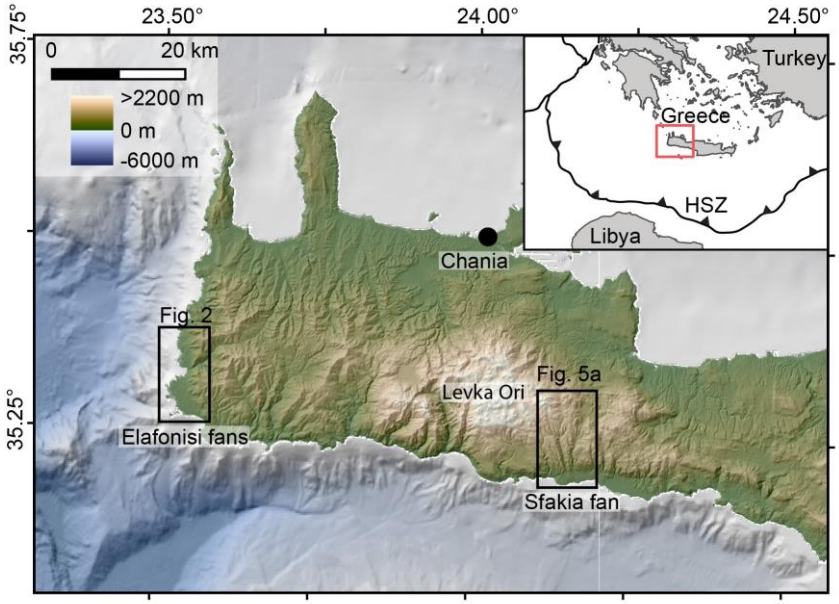

Fig. 1. Overview of the study sites in western Crete, Greece. Inset location of western Crete within the Hellenic Subduction Zone (HSZ).

2 Background

Crete occupies a forearc high within the Hellenic Subduction Zone, where the African Plate subducts beneath the Aegean Plate at a rate of ~ 35 mm/a (Reilinger et al., 2006, 2010). Most of Crete is part of a nappe pile stacked during mid-Cenozoic subduction and exhumed during subsequent extensional deformation in the late Cenozoic (Fassoulas et al., 1994; Jolivet and Brun, 2010). The Sfakia fan is a ~ 3.2 km² large telescopic fan, and the westernmost of seven coalesced fans (Nemec and Postma, 1993). The 24 km² large catchment sourcing the Sfakia fan consists

mostly of platy limestones with interbedded cherts of the Jurassic to Eocene Plattenkalk formation and limestone of the Jurrasic Trypali unit (Creutzberg et al., 1977). The Elafonisi fan system consists of eight adjacent alluvial fans along the southwestern coast of Crete. We collected samples along the Stomio River, which drains the largest (35 km²) catchment of the Elafonisi area and has several river terraces preserved near its outlet. Additionally, we sampled two ~ 1.5 km² catchments with telescopic fans near Livadia and Chrissoskalitissa (Fig. 2). The Stomio and Livadia catchments are dominated by the Carboniferous to Middle Triassic Phyllite-Quartzite (PQ) unit, whereas the Plattenkalk formation is exposed in the Chrissoskalitissa catchment.

The Elafonisi and Sfakia fans are situated at the coast and are sensitive to base-level changes in response to eustatic sea-level change and vertical crustal motion. Ott et al. (2019b) documented average uplift rates of ~ 1.2 mm/a since 71 ka at Elafonisi and < 0.1 mm/a since 125 ka for the hanging wall of the Sfakia fault on which the fan is deposited. The Krios paleoshoreline, which can be traced along the western coast of Crete, documents Late Holocene uplift during either a single (Shaw et al., 2008) or a sequence of earthquakes (Ott et al., 2021) by about 8 m at Elafonisi and 2.9 m at Sfakia (Angelier, 1979; Ott et al., 2021). However, on a Late-Pleistocene timescale, rock uplift rates along the coast of Crete are relatively steady (Strasser et al., 2011; Gallen et al., 2014; Ott et al., 2019b; Robertson et al., 2019).

In contrast to the Elafonisi fans, the Sfakia fan has been studied in detail for its sedimentology and depositional history. Two main units can be distinguished (Nemec and Postma, 1993; Pope et al., 2008, 2016), which we refer to as Quaternary deposit (Qt) 1 and Qt2. Qt1 is only preserved at the head of the Sfakia fan and is dominated by thick beds of subangular to subrounded, cobble-to-boulder-sized clasts, interpreted as debris-flow deposits (Nemec and Postma, 1993; Pope et al., 2008). Unit Qt2 is inset into Qt1 and consists of better-sorted, pebble to cobble streamflow deposits with interspersed debris-flow layers. Both fan units contain layers of fine-grained red silt with angular pebbles and lenses of pale tan silt, which represent paleosols and small dune deposits, respectively (Nemec and Postma, 1993). For a more detailed description of the sedimentology of the Sfakia fan, we refer the reader to Nemec and Postma (1993) and Pope et al. (2008). Based on published geochronologic ages, Qt1 was deposited mainly during MIS 5, and after a brief period of incision at the beginning of MIS 4, Qt2 was deposited from MIS 4 to MIS 2 (Pope et al., 2008, 2016). Qt2 is now deeply incised; based on archaeological evidence, the incision must have started before about 5.5 ka (Pope et al., 2008).

Today, both catchments are dominated by a hot-summer Mediterranean climate (*Csa* in the Köppen-Geiger climate classification) (Beck et al., 2018). The mean annual precipitation for the Elafonisi and Sfakia catchments is 817 and 656 mm/a, respectively. The lower precipitation rate and reduced water-holding capacity of the limestone terrain dominating the Sfakia catchment likely explains its lower vegetation density than the Elafonisi area (Ott, 2020). Eastern Mediterranean climate during the last glacial cycle was characterized by cold and dry stadials (MIS 2, 4, 6) and comparatively warm and wet interglacials and interstadials (MIS 1, 3, 5) (Cheddadi and Rossignol-Strick, 1995; Langgut et al., 2011). A potential glaciation of the Levka Ori Mountains above the Sfakia catchment remains debated (Hughes and Woodward, 2017).

Nevertheless, even if small glaciers existed in the Levka Ori Mountains, the Sfakia catchment presently lacks surficial streams connecting the fan to the highest areas of the Levka Ori. Hence, a direct influence of glacial processes on fan evolution is unlikely, but cannot be ruled out.

Catchment-wide denudation rates on Crete have been determined from the PQ unit in western Crete and carbonate catchments throughout the island (Ott et al., 2019a). ^{10}Be-derived denudation rates in western Crete are around 0.11 mm/a, and ^{36}Cl-derived denudation rates from carbonate areas average 0.13 mm/a (Ott et al., 2019a). Ott et al. (2019a) concluded that the carbonate massifs and PQ mountains in western Crete denude at similar rates but that infiltration of precipitation into the karst system causes the carbonate mountains to form steeper topography despite experiencing similar uplift rates.

3 Materials and Methods

We built on the existing geochronological framework established by 39 luminescence and U-Th ages from the Sfakia fan (Pope et al., 2008, 2016) and collected samples for paleo-denudation rates from dated and rapidly-buried layers. For the previously-undated Elafonisi fan system, we established the geochronology using luminescence and radiocarbon dating. Samples for paleo-denudation rates were taken from sedimentary layers with age control, and either ^{36}Cl or ^{10}Be concentrations were measured depending on the sediment source.

3.1 Field mapping and digital elevation data

The redness of soil B-horizons in arid landscapes is related to the concentration of secondary iron oxides and has been used extensively for relative age determination of alluvial fan surfaces (Harvey et al., 1999; Ferrier and Pope, 2012). B-horizon soil redness was determined on the fine-grained matrix between clasts using a Munsell colour chart. Mapping of the Quaternary (Qt) units is based on soil redness, geomorphic position (elevation), observed unconformities, and abrupt changes in fan surface slope. At the Sfakia fan, we used a drone for aerial images and built a digital elevation model (DEM) using photogrammetric software (Agisoft). At Elafonisi, a 5m DEM was provided by the Hellenic Cadastre SA. For mapping marine paleoshorelines, the inner shoreline angle (ISA) was estimated in the field, and its elevation was measured with a laser range finder. ISA refers to the intersection point between the abrasion platform and the paleo-sea cliff and approximates the paleo-sea level during paleoshoreline formation (Lajoie, 1986).

3.2 Optically Stimulated luminescence (OSL)

We collected seven samples from fan and river terrace deposits within the Elafonisi study area to constrain the timing of sediment deposition and burial by OSL measurements (Tab.1). Samples were collected in light-proof metal cylinders driven 0.25 m horizontally into fine-grained sedimentary lenses. In addition, moisture samples were collected in an airtight plastic container, and environmental dose rate samples were collected by representatively capturing sediment from a ~30 cm radius surrounding the OSL sample.

OSL samples were analysed by single-aliquot regenerative-dose (SAR) procedures for dating quartz sand (Murray and Wintle, 2000; Wintle and Murray, 2006) at the Utah State University Luminescence Laboratory, Logan, UT, USA, following standard procedures involving safelight conditions, sieving, gravity separation, and acid treatments with HCl and HF to isolate the quartz component of the 90-150 μm grain-size range following procedures outlined in Aitken (1998) and described in Rittenour et al. (2003, 2005). Samples were analysed on Risø OSL/TL DA-20 luminescence readers with blue-green (470 nm, 36 W/m^2) stimulation and detection through 7.5-mm UV filters (U-340). Stimulation was conducted at 125°C following 240°C preheats (10s) for regenerative and natural doses. Dose-response curves were created using five sensitivity-corrected regenerative-dose points (including a repeat and zero-dose step). The resultant data were fit with a saturating exponential curve from which the equivalent dose (D_E; reported in Figure S1) is determined. The D_E, reported in Table 1, is based on a central age model (Galbraith and Roberts, 2012) from the measurement of at least 20 aliquots of sand mounted on a two mm-diameter area of the measurement disks (~200 grains/aliquot). Dose-rate measurements were determined by chemical analysis of the U, Th, K, and Rb content using ICP-MS and ICP-AES techniques and conversion factors (Guérin et al., 2011). The contribution of cosmic radiation to the dose rate was calculated using sample depth, elevation, and latitude/longitude following Prescott and Hutton (1994). Sediments were dry when collected, but a value of 3 ± 3 wt% water content was thought to be representative of burial history. Total dose rates were calculated based on water content, radioisotope concentration, and cosmic contribution (Adamiec and Aitken, 1998; Aitken, 1998).

3.3 Radiocarbon dating

To constrain the end of the last depositional phase at the Sfakia fan, we dated carbonate rinds (thickness of 1 – 5 mm) from the upper meter of a coastal cliff at the distal end of the Sfakia fan (Tab. 2). The dating of carbonate cement has been utilized in similar studies to constrain the timing of cementation periods, thereby providing a minimum depositional age (Geyh and Eitel, 1997; Giresse and Martzluff, 2015). All samples were leached with 0.5 M HCl to remove possible surface contamination, put in 12 ml septum sealed vials (Labco), flushed with helium, dissolved with H_3PO_4 (85%), and converted to graphite targets using automated graphitization equipment (Synal et al. 2007). Accelerator Mass Spectrometry (AMS) was carried out at the Laboratory for IonBeam Physics at ETH Zürich using a Mini Carbon Dating System (MICADAS) AMS (Synal et al., 2007). Oxalic acid II NIST standard was used for fractionation correction and standard normalization. Radiocarbon ages were converted with IntCal 20 (Reimer et al., 2020) to calendar years.

Additionally, we dated a terrestrial gastropod (snail) shell sampled from a silt layer contained within a channel incised into the fan surface at the Chrissoskalitissa site to constrain the timing of fan-surface abandonment and the onset of incision (Tab.1, Fig. 3G). After sieving bulk sediment and microscopic examination, a single, intact shell was selected. The shell was broken and cleaned in milli-Q water with sonic vibration before removing the outer surfaces with dilute HCl. This sample was analysed at the University of California Irvine Keck Carbon Cycle AMS Facility

(UCIAMS), following standard cleaning and preparation techniques. The reported radiocarbon age was corrected for isotopic fractionation according to Stuiver and Polach (1977), and sample preparation backgrounds were subtracted based on measurements of ^{14}C-free calcite. The sample δ^{13}C value was measured relative to standards traceable to Pee Dee Belemnite, using a Thermo Finnigan Delta Plus stable isotope ratio mass spectrometer with Gas Bench input.

3.4 Cosmogenic nuclide measurements

We analysed 11 cosmogenic nuclide samples to determine (paleo-)denudation rates. For three samples sourced by the quartz-rich PQ unit (Stomio River and Livadia at Elafonisi), we measured only ^{10}Be on quartz (Tab. 3). In the carbonate sediments from the Chrissoskalitissa fan, we measured only ^{36}Cl concentrations on calcite. For five samples from the Sfakia fan, we measured ^{36}Cl concentrations on calcite and ^{10}Be on cherts to test if denudation rates from both nuclides agree. To compare Holocene denudation rates with rates of paleo-denudation during the Late Pleistocene, we also measured cosmogenic nuclide concentrations in modern stream sediment. At the Elafonisi site, a ^{10}Be concentration from modern sediments in the Stomio River was published by Ott et al. (2019a) (location in Fig.2).

3.4.1 ^{36}Cl measurements

We collected sediment samples with grain sizes between 1 – 4 mm, for consistency with ^{36}Cl catchment-wide denudation rate measurements by Ott et al. (2019a). The samples were crushed to <1 mm with a disc mill, after which we separated the fraction for ^{10}Be measurement on cherts from the Sfakia fan samples. Meteoric ^{36}Cl was removed by repeated etching with 2M HNO_3 and rinsing with milli-Q water. A ^{35}Cl spike (Ivy-Ochs et al., 2004) was added to the samples before their dissolution with HNO_3 (Prager et al., 2009). The samples were measured at the 6MV TANDEM AMS at ETH Zurich, which utilizes a gas-filled magnet to separate the ^{36}S isobar (Vockenhuber et al., 2019), and were calibrated using the internal K382/4N standard (Christl et al., 2013) (Tab. 3). The chemical composition of the ^{36}Cl samples was determined with an ICP-MS for both the bulk sample and the undissolved remnants to determine the composition of the bulk sample and the dissolved target mineral. The compositional data for bulk rock and target minerals is reported in Table S1.

3.4.2 ^{10}Be measurements

In the northern Elafonisi area, we collected three samples of sand and processed the 0.25 – 0.71 mm size fraction for ^{10}Be analysis. We separated quartz from other minerals by magnetic separation and repeated etching with hydrochloric, hydroflourosilicic, and hydrofluoric acid. A ^{9}Be carrier was added, and Beryllium was extracted using ion chromatography (Bierman et al., 2002). The ^{10}Be/^{9}Be isotope ratios were measured by the 500kV TANDY Accelerator Mass Spectrometer (AMS) at ETH Zurich and calibrated using the S2007 N ^{10}Be standard (Christl et al., 2013) (Tab. 3). The five chert samples from the Sfakia fan were cleaned by etching with hydrochloric and nitric acid and measured at the Cologne AMS (Dewald et al., 2013) relative to standards KN01-6-2 and KN01-5-3.

3.5 Post-burial production and (paleo-) denudation rate calculations

We calculated (paleo-) denudation rates with the CRONUScalc v2.1 tools (Marrero et al., 2016a). However, we modified the scaling factor functions (scalefacs1026, scalefacs36) to calculate scaling factors based on a pixel-by-pixel approach for the entire catchment area. Catchment scaling factors were calculated on a 30-m SRTM Digital Elevation Model (DEM) for modern and paleo-denudation rates. Time-dependent production rates were calculated with the Stone (2000) scaling and accounting for geomagnetic variations after Nishiizumi et al., (1989). We assume a bulk density of 2.65 g/cm³ and 2.2 g/cm³ for the bedrock and fan deposits (Rodés et al., 2011), respectively, with an uncertainty of 0.1 g/cm³.

We developed a Monte Carlo routine that utilizes the CRONUScalc v2.1 production rate functions to estimate Post-burial Production ("PostPro") (Ott, 2022). First, the age of the sampled layer and age constraints on layers above are used to build a time-depth history, assuming that aggradation between two layers of known age occurred at a constant rate. Then, for each paleo-denudation sample, we generated 5000 synthetic time-depth histories by randomly drawing an age and depth for each dated layer, assuming normally distributed ages and depths defined by the geochronologic ages, measured depths, and their respective uncertainties. In addition, for every simulation, production rates are drawn from normal distributions with uncertainties of 8% in ^{10}Be spallation production (Phillips et al., 2016), 30% in muon production (3 times the value of Phillipps et al., 2016, to avoid underestimation of the uncertainty), and ^{36}Cl production rate uncertainties based on Marrero et al., (2016b) (for spallation and muon production we use the average of the relative uncertainties in the dominating Ca and K production). Subsequently, post-depositional production and decay are computed for every synthetic burial history. The mean post-depositional nuclide concentration from the sampled layer is then subtracted from the measured concentration, and the uncertainty in post-burial production is propagated together with the AMS and blank correction uncertainty. A link to the PostPro code can be downloaded at https://github.com/Richard-Ott/PostPro with example input from this study.

The computation of post-burial production requires an age for the end of above-sample deposition. In most sampled locations, we used the mean of the age of the youngest deposited layer and the oldest incision constraint, which often corresponds to the depositional age of the next younger unit. However, at the Sfakia fan and a Stomio River terrace (Elafonisi), we also report an alternative scenario based on less conservative assumptions of surface abandonment. The analysis presented in the main text is based on the more conservative estimates for surface abandonment ages listed in Table 4. We report a detailed description of constraints on surface abandonment and uncertainty calculation in Table S2. Table S3 documents the results for the alternative burial scenario.

4 Results

4.1 Elafonisi fan

4.1.1 Depositional chronology

At the Elafonisi fan system, four units of Quaternary deposits (Qt) can be identified (Fig. 2). These units are bounded by erosional unconformities and inset into each other. Qt1 consists of a steep (10°), cobble-dominated fan in the highest geomorphic position on the Livadia fan (Fig. 2). The high soil redness (2.5YR 4/8 to 2.5YR 3/6, red to dark red), the elevated geomorphic position, and the deep incision of Qt1 suggest a relatively old formation age (Fig. 3B). Unit Qt2 is deposited along the Stomio River and its outlet (Fig. 2). Qt2 forms a continuous river terrace 60-70 m above the stream (Fig. 3A) of well-cemented, poorly to moderately-well sorted fluvial sediments of sand to boulder size (Fig. 3F). Qt3 is inset into Qt2 at the mouth of the Stomio River (Fig. 3A) and Qt1 at the Livadia fan (Fig. 3B). At the Livadia fan, Qt3 is characterized by cobble-dominated, poorly-sorted fan deposits of red soil colour (2.5YR 4/8), with some thinly (~10 cm) bedded silt to sand-sized lenses. Closer to the mouth of the Stomio River, Qt3 is strongly cemented and consists of coarser grains ranging from sands to boulders (Fig. 3D). The gradient of the Qt3 fan surface (6°) is substantially lower than the Qt1 fan surface. Qt4 is inset into the Qt3 fan at the Livadia fan and exhibits similar sedimentology but significantly lower soil redness (2.5YR 6/4 – light reddish-brown). At the Chrissoskalitissa fan, a water reservoir is cut into a Qt4 fan surface and exposes ~20 m of weakly bedded, poorly-cemented sand to cobble-sized clasts (Fig. 3G) with similarly low soil redness. Across all Qt units, the average grain size appears greatest along the Stomio River and its outlet. Strong cementation of units along the Stomio River deposits points to an admixture of the Plattenkalk unit's carbonates.

All mapped Qt units are currently being incised. Their stratigraphic relationships, cross-cutting, and differences in soil redness confirm a relative sequence of events starting with deposition of Qt1 and ending with Qt4, with periods of incision separating the individual aggradation events.

Several paleoshoreline levels are cut into the bedrock and Qt units, documenting long-term rock uplift. Four paleoshoreline deposits with inner shoreline angles (ISA) ranging in elevation from 8 to 53 m have been identified (Fig. 2). These deposits are found on bedrock straths (Fig. 3E) or erosional surfaces and along cliffs within the Qt deposits. In addition, marine deposits crop out near the coastline (Fig. 2) and have previously been assigned a Miocene to Pliocene age (Mountrakis et al., 2012), albeit with poor age control. This marine formation consists of unsorted cobbles, pebbles, and sand derived from the PQ unit, mixed with algal constructions in a matrix-dominated well-cemented carbonate rock (Fig. 3C). We interpret these deposits as the subaqueous part of the Stomio River delta system that has been uplifted above sea level and refer to this unit as the Stomio Formation.

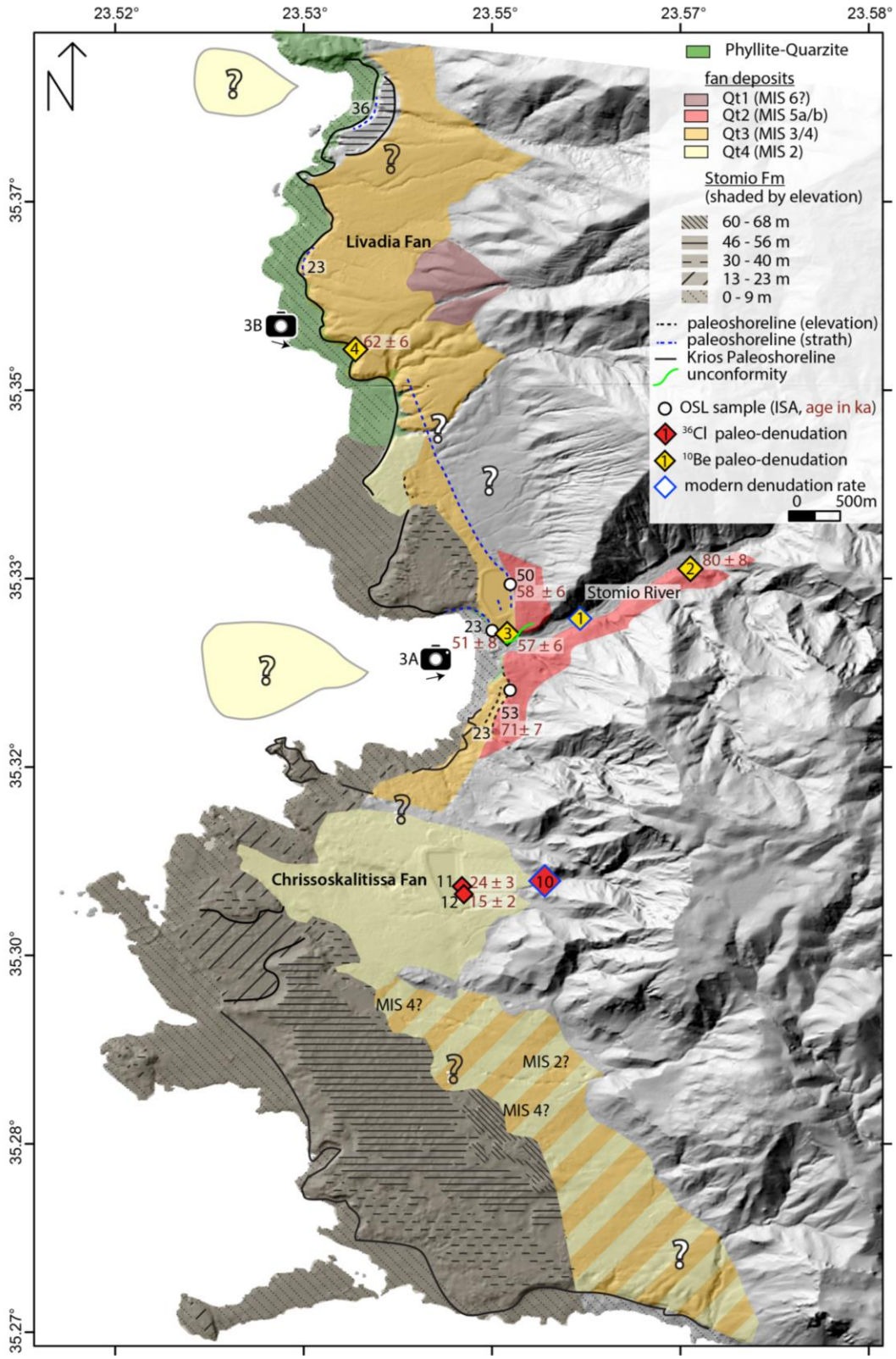

Fig. 2. Elafonisi mapping results and geochronology. Numbers for denudation rate samples correspond to Table 4. In addition, for paleoshorelines, the elevation of the inner shoreline angle (ISA) is indicated.

Fig. 3. Field pictures from Elafonisi fan system. See Figure 2 for image locations. (A) View of the Stomio River mouth. For visibility, the 23 m paleobeach strath and deposit is highlighted in yellow. (B) View of the Livadia fan. (C) Marine deposit of the Stomio Formation containing cobbles, pebbles, and algal constructions. (D) Close up of unit Qt3. (E) Paleobeach deposited on strath in gypsum bedrock. (F) Dated channel in Qt2 deposit. (G) Dated section of the Chrissoskalitissa fan. The white circles are OSL samples; the yellow circle is a radiocarbon sample of a fill deposit inset into the Qt4 fan.

4.1.1.1 New chronological constraints

Our seven luminescence ages range from approximately 81 to 15 ka and show a younging trend with lower (inset) topo-geomorphic positions (Table 1), which agrees with the relative deposition sequence established by field observations. A 15 m wide channel cross-section from ~20 m below the top of the Qt2 deposit (Fig. 3F) was dated to 80 ± 8 ka. At the Livadia fan, a sample 10 m below the Qt3 fan surface returned an age of 62 ± 6 ka. Near the mouth of the Stomio River, Qt3 was dated to 57 ± 8 ka, 3 m below the deposit surface. Aggradation of the Chrissoskalitissa fan is constrained by the age of 24 ± 4 ka near the bottom, and 15 ± 2 ka, 3 m below the fan surface. The switch from aggradation to subsequent incision at Chrissoskalitissa is constrained by a radiocarbon age from a snail shell within the channel that incised the fan to 11.3-11.2 ka (2σ range) (Fig. 3G). Two paleoshorelines near the Stomio River mouth, with ISAs of 53 m and 23 m, were dated to 58 ± 6 and 51 ± 8 ka, respectively.

4.1.1.2 Synthesis of new and published chronological data

Our new geochronologic ages and published observations constrain the timing of aggradation and incision at Elafonisi (Fig. 4). Our luminescence age of Qt2 suggests deposition around MIS 5a/b. A paleoshoreline forming a paleocliff in Qt2 south of the Stomio River mouth was dated to 71 ± 7 ka (Ott et al., 2019b) and potentially marks the incision into Qt2. However, we dated a paleoshoreline at the same elevation to 58 ± 6 ka north of the Stomio River mouth. Both ages overlap within uncertainty, yet paleoshorelines on Crete have been shown to form during sea-level high stands (Gallen et al., 2014; Ott et al., 2019b; Robertson et al., 2019). Therefore, we assume the 71 ± 7 ka age lies closer to the true age because it matches the MIS 5a highstand, commonly preserved on Crete (Ott et al., 2019b). A paleoshoreline dated to 51 ± 8 ka and inset against Qt3 serves as an incision constraint of Qt3 aggradation, which occurred at ~60 ka. Aggradation of Qt4 occurred during MIS 2 based on our two luminescence ages from Chrissoskalitissa, and incision of Qt4 commenced about 11 ka.

Table 1. Luminescence age information from the Elafonisi fan area.

Sample	Lab-ID	Grain size (μm)	Num. of aliquots[†]	Dose rate[‡] (Gy/kyr)	Equivalent Dose (D_E)[§] ± 2σ (Gy)	OSL Age ± 1σ (ka)
KWW-102508-5	USU-485	90-150	23 (50)	1.42 ± 0.07	81.97 ± 9.31	**57.81 ± 5.90**
KWW-102408-1A	USU-486	90-150	29 (57)	0.73 ± 0.04	17.28 ± 2.53	**23.74 ± 2.73**
KWW-102408-1D	USU-487	75-150	36 (49)	0.97 ± 0.05	14.38 ± 1.66	**14.75 ± 1.53**
KWW-102408-2	USU-488	90-150	24 (55)	1.72 ± 0.08	138.16 ± 15.39	**80.29 ± 8.05**
KWW-102508-2	USU-489	75-150	28 (57)	1.54 ± 0.07	87.37 ± 9.73	**56.81 ± 7.88**
KWW-102508-2	USU-490	63-125	26 (69)	1.89 ± 0.08	96.36 ± 12.49	**50.92 ± 7.82**
062009-1	USU-600	75-150	31 (60)	1.83 ± 0.08	112.80 ± 11.12	**61.67 ± 5.98**

[†] Age analysis using the single-aliquot regenerative-dose procedure of Murray and Wintle (2000) on 2-5 mm small-aliquots of quartz sand. Number of aliquots used in age calculation and number of aliquots analyzed in parentheses.

[‡] Assumed 3.0 ± 3.0% as moisture content over burial history.

[§] Equivalent dose (D_E) calculated using the Central Age Model (CAM) of Galbraith and Roberts (2012).

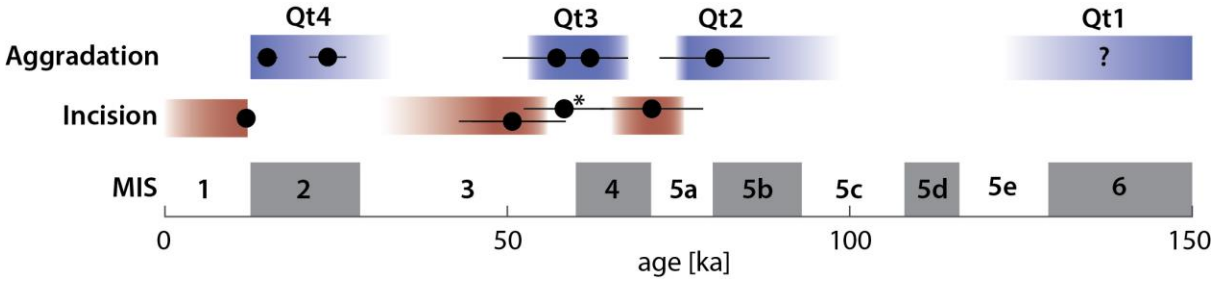

Fig. 4. Elafonisi aggradation (blue) and incision (red) constraints versus marine isotope stadial and interstadial extents since 150 ka. The asterisk (*) indicates an OSL sample age from a paleoshoreline excluded from the geochronologic interpretation (see text).

4.1.2 Uplift rates

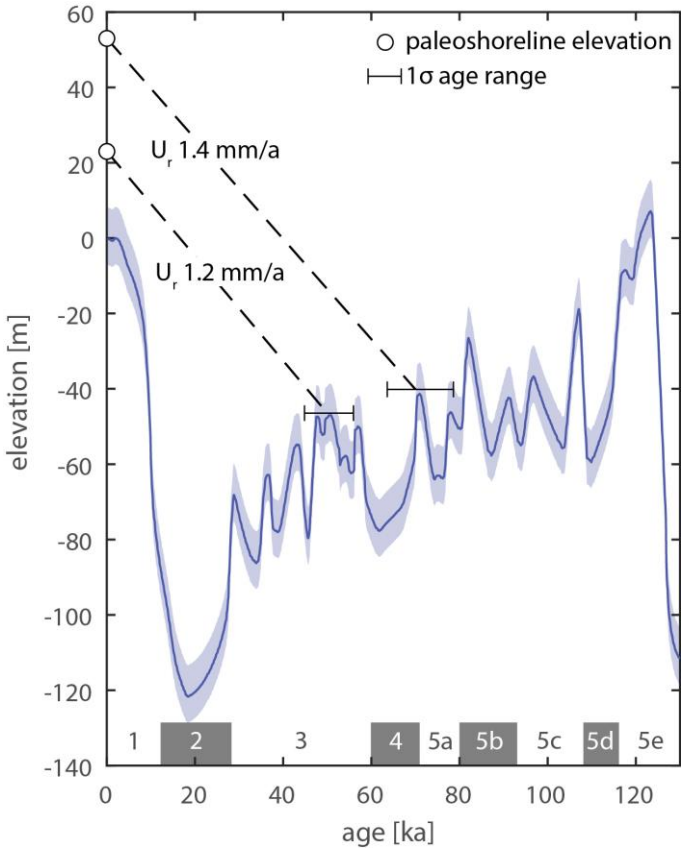

Fig. 5. Sea level correlation for the two dated paleoshorelines at the Elafonisi area using the eustatic curve of Lambeck & Chappell (2001)*. Dashed lines indicate the rock uplift rates based on sea-level highstand correlations. Marine isotope stages are highlighted along the x-axis.*

We dated two uplifted paleoshorelines at the Elafonisi site. The correlation of the paleoshorelines with eustatic sea-level highstands (Lambeck and Chappell, 2001) allows for calculating time-averaged uplift rates of 1.2 and 1.4 mm/a (Fig. 5). Long-term uplift is also exemplified by the five different marine abrasion platforms cut into the Stomio Fm. Platforms with elevations ranging

from 46 to 56 m likely correlate with our paleoshorelines mapped at 53 m, platforms with elevations of 13 to 23 m probably correspond to the paleoshoreline mapped at 23 m elevation, and platforms between 0 and 9 m are linked to the historic uplift in the first centuries AD.

4.2 Sfakia fan depositional chronology

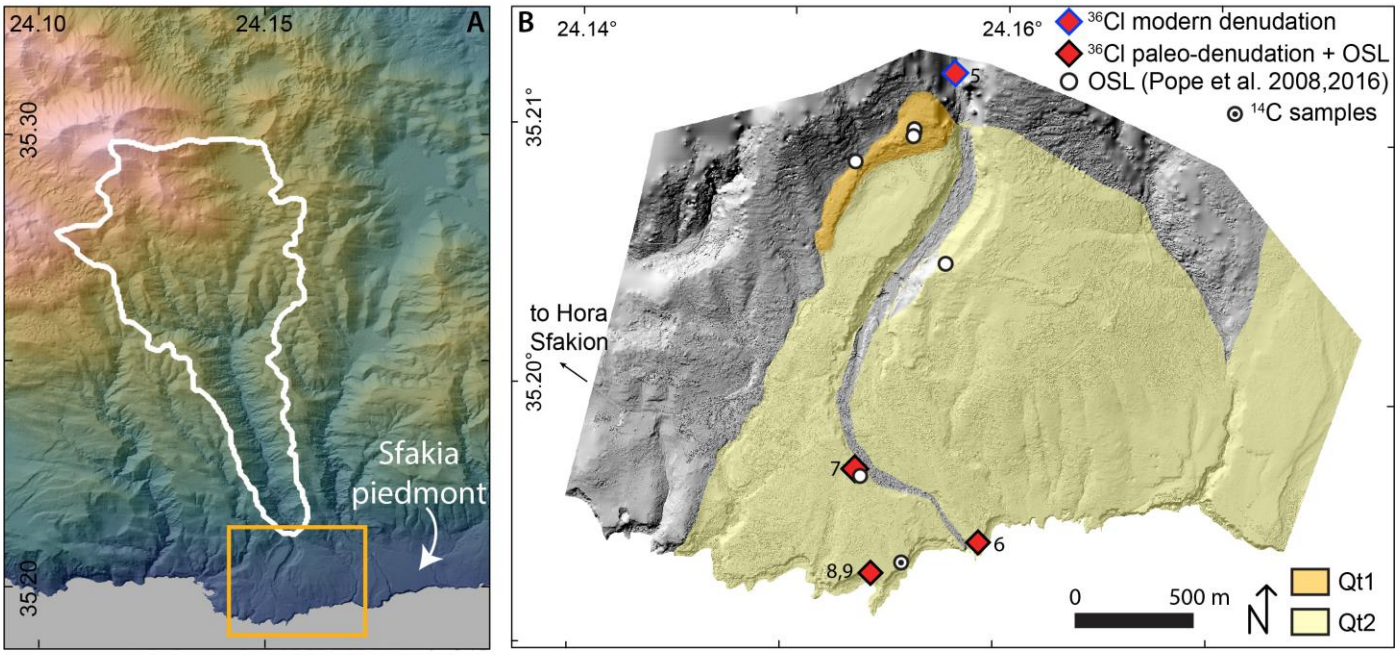

Fig. 6. (A) Topography of Sfakia catchment with the box outlining the extent of (B). (B) Overview of Sfakia fan and sampling locations. The numbers of denudation rate samples correspond to Tab. 4.

As mentioned in section 2, published geochronologic ages from the Sfakia fan show Qt1 deposition during MIS 5 and, after a short period of incision, Qt2 deposition from MIS 4 to MIS 2 (Pope et al., 2008, 2016) (Fig. 6). Currently, both units are being incised by the active channel, with up to 45 m of incision into Qt2 (Fig. 7A, C). Incision commenced between 5.5 and 11.2 ka (Pope et al., 2008) and we dated nine carbonate cement rinds from the uppermost distal section of the fan (Figs. 6, 7D) to improve these estimates. The calibrated age ranges show a large spread from 3.7 to 11.1 ka (Tab. 2). The spread in ages is likely related to multiple periods of cement formation and uncertainty in cement carbon source (Geyh and Eitel, 1997). We use the oldest cement ages as an estimate of fan surface abandonment in our alternative burial scenario (supplement), but apply the conservative 5.5-11.2 ka Qt2 abandonment time range for the postburial correction of Sfakia paleo-denudation samples.

Fig. 7: Sfakia fan images and sampling locations. (A) Overview of fan head with Qt1 unit outlined by the dashed line, and inset Qt2 fan deposits. (B) Sea cliffs eroded into the distal Qt2 fan deposits. (C) 45 m thick section of Qt2 stratigraphy exposed in deeply incised feeder channel. (D) Carbonate clasts in the fan deposit are cemented by brown calcite cement, which we used for radiocarbon dating. (E) Section dated by Pope et al., (2008). Note hammer for scale. (F) Sea cliff in the Qt2 fan. The base of this section is shown in (E).

Tab. 2: Radiocarbon data from the Sfakia and Elafonisi fans.

Sample	Lad-ID	°N	°E	$\delta^{13}C$	^{14}C age BP	calBP (2σ)	dated material
1A	105011.1.1	35.19327	24.15583	-12.69	4699 ± 78	5593 - 5290	carbonate rind
1B	105012.1.1	35.19327	24.15583	-10.10	5235 ± 74	6266 - 5765	carbonate rind
1C	105013.1.1	35.19327	24.15583	-8.75	8486 ± 82	9658 - 9283	carbonate rind
1D	105014.1.1	35.19327	24.15583	-13.35	9475 ± 87	11107 - 10507	carbonate rind
2A	105015.1.1	35.19327	24.15583	-20.12	3960 ± 72	4786 - 4155	carbonate rind
2B	105016.1.1	35.19327	24.15583	-15.44	4018 ± 76	4816 - 4254	carbonate rind
2C	105017.1.1	35.19327	24.15583	-14.79	6351 ± 79	7428 - 7027	carbonate rind
2D	105018.1.1	35.19327	24.15583	-17.07	3575 ± 73	4086 - 3650	carbonate rind
2E	105019.1.1	35.19327	24.15583	-6.59	5590 ± 77	6558 - 6214	carbonate rind
3	UCIAMS-68078	35.30571	23.54750	-7.5	9910 ± 20	11394 - 11243	terrestrial snail shell

4.3 Paleo-denudation rates

Tab. 3: ^{10}Be and ^{36}Cl AMS results.

Sample	AMS code	Lat (°)	Lon (°)	Elevation (m)	$^{10}Be/^{9}Be$	Error (%)		Carrier (mg)	Weight (g)	^{10}Be (at/g)
^{10}Be										
El-919-1	ZB7493	35.33412	23.56767	96	3.23E-14	9.3%		0.2456	13.72	34200 ± 5000
El-919-2	ZB7494	35.32846	23.55132	34	3.84E-14	6.9%		0.2507	16.37	35500 ± 4000
El-617-PE-4	TB3908	35.35393	23.53772	48	4.22E-14	8.7%		0.247	35.33	15600 ± 2400
SF-919-1†	s16955	35.21184	24.15585	220	1.05E-13	5.28		0.161	44.75	24353 ± 1441
SF-919-11†	s16956	35.19444	24.15918	18	1.13E-13	4.93		0.163	33.26	35787 ± 1972
SF-919-12†	s16957	35.19665	24.15364	67	1.41E-13	4.82		0.146	48.48	27667 ± 1444
SF-919-14†	s16958	35.19306	24.15426	24	3.41E-13	3.93		0.163	60.64	60546 ± 2439
SF-919-15†	s16959	35.19306	24.15426	24	1.33E-13	5.23		0.138	44.03	27158 ± 1537
Sample	AMS code	Lat (°)	Lon (°)	Elevation (m)	$^{36}Cl/^{35}Cl$	Error (%)	Cl (ppm)	Carrier (mg)	Weight (g)	^{36}Cl (at/g)
36Cl										
EI-919-3	CV3829	35.30663	23.55487	174	2.31E-14	10.11	236.3 ± 1.6	3.653	63.36	76000 ± 12317
EI-919-4	CV3830	35.30588	23.54728	96	3.07E-14	7.45	312.2 ± 1.8	3.692	67.95	131000 ± 14876
EI-919-5	CV3831	35.30588	23.54728	106	2.37E-14	8.63	299.8 ± 2.1	3.658	66.06	93000 ± 13546
SF-919-1	CV3832	35.21184	24.15585	220	1.12E-13	5.67	23 ± 2.3	3.668	41.62	195000 ± 12030
SF-919-11	CV3833	35.19444	24.15918	18	1.26E-13	5.04	18.1 ± 2	3.666	43.30	205000 ± 11195
SF-919-12	CV3834	35.19665	24.15364	67	1.17E-13	5.22	15.8 ± 2	3.671	39.50	202000 ± 11496
SF-919-14	CV3835	35.19306	24.15426	24	1.07E-13	5.62	25.7 ± 29.1	3.673	24.37	298000 ± 18343
SF-919-15	CV3836	35.19306	24.15426	24	1.14E-13	4.91	18 ± 0.9	3.675	42.66	187000 ± 10097

Average blank ratios for corrections ^{10}Be (Cologne) 3.4E-15 ± 2.3E-15, ^{10}Be (Zürich) 7.2E-15 ± 8.2E-16, ^{36}Cl 4.5E-15 ± 1.9E-15

†*measured at Cologne AMS*

We estimate post-burial production for all cosmogenic nuclide samples (Fig. 8, Tab. 3, Figs. S2, S3) to calculate paleo-denudation rates. For most samples, our estimated post-burial production is < 30% of the total concentration; only for sample Sf-919-12, we estimate that 44% of the measured ^{10}Be and nearly half of the measured ^{36}Cl concentration can be explained by production after deposition (Fig. 8, Tab. 4). For samples El-919-3 and El-919-4 from the Chrissoskalitissa fan, the post-burial ^{36}Cl production is probably high, but the uncertainties are large due to the high concentration (~ 300ppm) of natural Cl. The calculation of post-burial production with our alternative burial scenarios shows that the difference in the final concentrations is less than 10% (Tab. S3).

Tab 4. Post-burial production estimates and paleo-denudation rates. The numbers in the first column correspond to the location numbers in figures 2 and 5.

#	Sample	Model surface age (ka)	Postburial estimate (at/g)	Corrected ^{10}Be (at/g)	Erosion rate (mm/ka)
^{10}Be					
1	WC-616-7†	0 ± 0	0 ± 0	37800 ± 2400	108 ± 10
2	EL-919-1	68.5 ± 12.6	4406 ± 2493	29794 ± 5587	136 ± 27
3	EL-919-2	53.8 ± 11.1	9702 ± 5676	25798 ± 6944	159 ± 44
4	El-617-PE-4	56.3 ± 10.2	4914 ± 2722	10686 ± 3629	343 ± 116
5	Sf-919-1	0 ± 0	0 ± 0	24353 ± 1441	264 ± 24
6	Sf-919-11	8.6 ± 2	3972 ± 1745	31815 ± 2633	200 ± 22
7	Sf-919-12	8.6 ± 2	12408 ± 1902	15259 ± 2388	414 ± 68
8	Sf-919-14	8.6 ± 2	2578 ± 990	57968 ± 2633	110 ± 9
9	Sf-919-15	8.6 ± 2	2584 ± 1047	24574 ± 1860	259 ± 26
^{36}Cl					
10	El-919-3	0 ± 0	0 ± 0	76000 ± 12317	866 ± 193
11	El-919-4	13 ± 1.7	72801 ± 36741	58199 ± 39638	1421 ± 807
12	El-919-5	13 ± 1.7	92157 ± 38625	843 ± 40932	0 ± 0
5	SF-919-1	0 ± 0	0 ± 0	195000 ± 12030	236 ± 20
6	SF-919-11	8.6 ± 2	31099 ± 11439	173901 ± 16005	266 ± 28
7	SF-919-12	8.6 ± 2	95997 ± 13720	106003 ± 17900	422 ± 74
8	SF-919-14	8.6 ± 2	23408 ± 7715	274592 ± 19899	182 ± 17
9	SF-919-15	8.6 ± 2	20337 ± 6894	166663 ± 12226	263 ± 24

†*sample measured by Ott et al. (2019)*

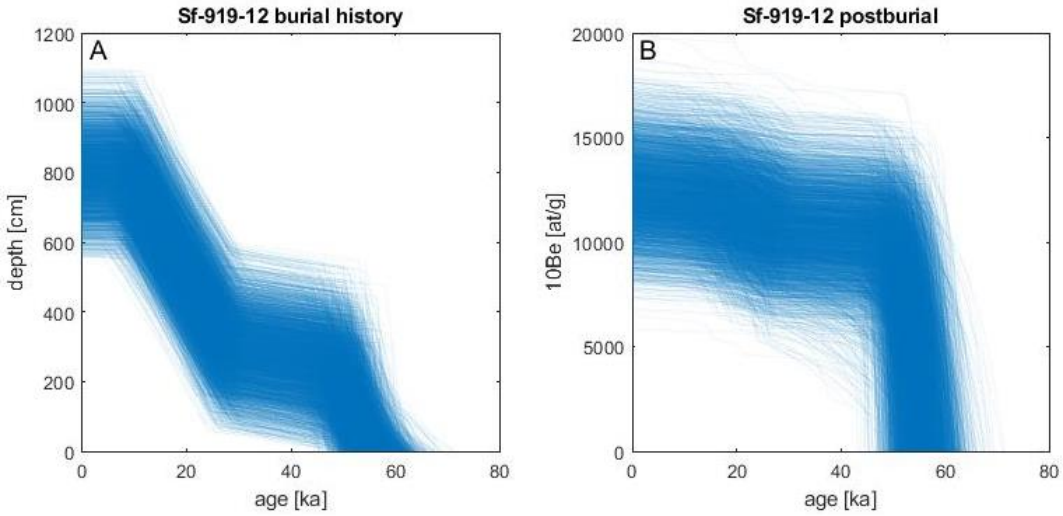

Fig. 8. Calculation of post-burial nuclide accumulation for sample Sf-919-12. (A) 5000 randomly sampled time-depth histories based on geochronologic ages and depth of overlying fan layers. (B) Forward models of nuclide accumulation due to post-burial production and radioactive decay calculated with PostPro and based on the time-depth paths in (A). Concentrations start at zero because only the nuclide accumulation after burial is shown.

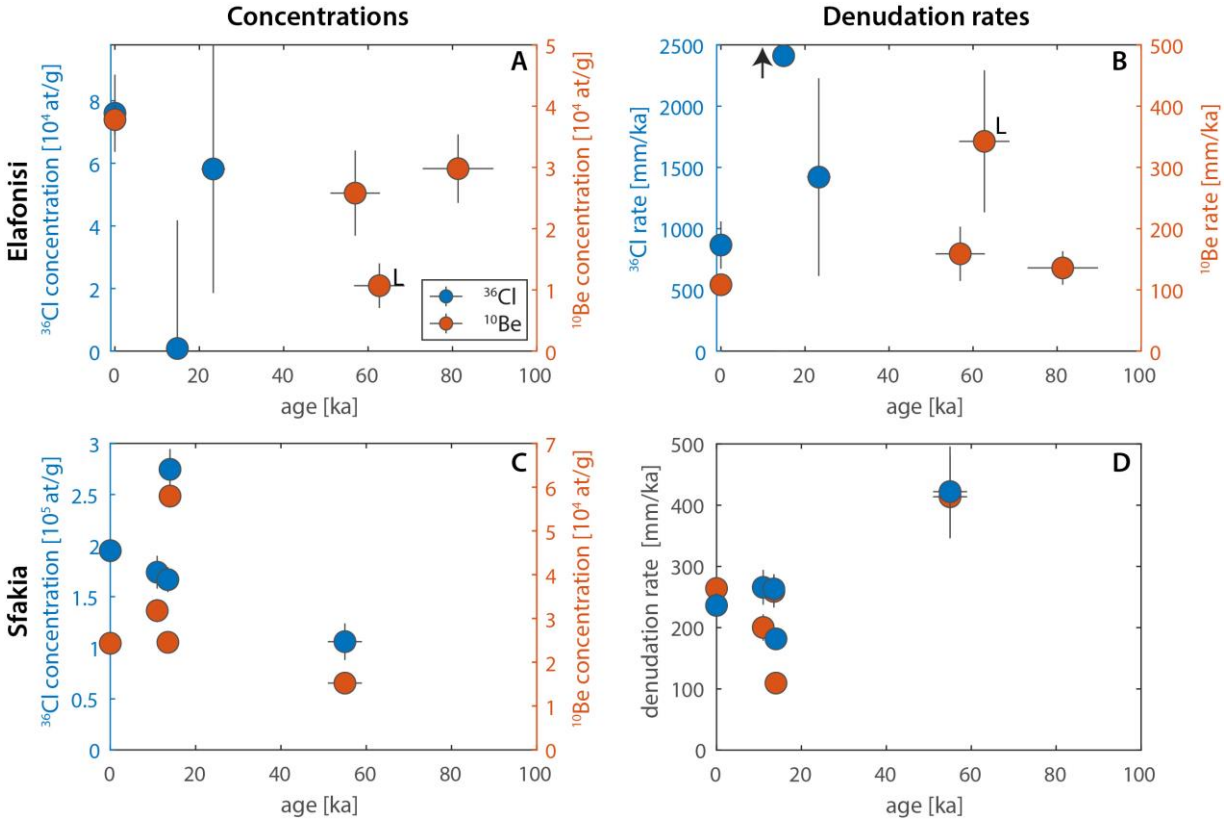

Fig. 9. Post-burial corrected concentrations and (paleo-) denudation rates from Elafonisi and Sfakia fans. L – Livadia fan. Note that one of the denudation rates in panel (B) from the

Chrissisoskalitissa fan could not be calculated because the concentration was too low. Therefore, the denudation rate is assumed to be high, as indicated by the arrow.

We calculated (paleo-)denudation rates from our post-burial-corrected concentrations (Tab. 4, Fig. 9). Denudation rates range from 108 mm/ka to 1421 mm/ka. At the Stomio River in the Elafonisi fan system, the modern denudation rate is 108 ± 10 mm/ka. Paleo-denudation rates are higher (136 ± 27 and 159 ± 44 mm/ka) but still overlap at one-sigma uncertainty. The paleo-denudation rate from MIS 4 at the Livadia fan system is higher (343 ± 116 mm/ka) but from a significantly smaller catchment (Fig. 2). At the Chrissoskalitissa fan, high concentrations of natural Cl cause large uncertainties in the post-burial production. The post-burial-corrected concentration of sample El-919-5 was too low for a denudation rate calculation. ^{36}Cl-derived paleo-denudation rates appear to be higher during MIS 2 compared to modern rates, yet due to the larger uncertainty in production rates, the modern and 23 ka paleo-denudation rates overlap within uncertainty.

At the Sfakia fan, most paleo-denudation rates are similar to modern rates, with some notable exceptions. The denudation rates from ^{10}Be and ^{36}Cl measurements agree for the modern stream sediment (264 ± 24 and 236 ± 20 mm/ka, respectively). However, three out of four ^{10}Be paleo-denudation rates are offset to lower values compared to the respective ^{36}Cl rates (Fig. 9). ^{10}Be-derived denudation rates are similar to or slower than modern rates during MIS 2 and were faster at the MIS 3/4 boundary. ^{36}Cl-derived denudation rates show the same pattern but are offset to larger values.

Nuclide accumulation during denudation predicts a ^{36}Cl/^{10}Be ratio that is dependent on the denudation rate and the sample-specific chemistry. We calculated the predicted ratios for a range of plausible denudation rates (50 to 500 mm/ka) and production parameter uncertainties (Fig. 10). Apart from the modern sample, all samples exhibit ^{36}Cl/^{10}Be ratios below the expected values. A prolonged deep sample burial can explain ratios larger than expected due to the greater percentage of muon production for ^{36}Cl. Alternatively, long and shallow (20-200 cm) sample material burial can reduce the ratio (~3.5 to 6 depending on sample composition). However, our independent constraints on aggradation and incision do not allow for significant burial at depths shallow enough to significantly reduce the ^{36}Cl/^{10}Be ratios. Another explanation for a low ^{36}Cl/^{10}Be ratio is the incomplete removal of meteoric ^{10}Be from our chert samples. It has previously been shown that adsorbed ^{10}Be can be challenging to remove from cherts and lead to an excess of ^{10}Be (Zerathe et al., 2013). In the absence of any other reasonable explanation, we assume that the incomplete removal of adsorbed ^{10}Be by the amorphous silicates led to the low ^{36}Cl/^{10}Be ratios. Therefore, we focus on the ^{36}Cl-derived denudation rates in our interpretation of the Sfakia fan evolution.

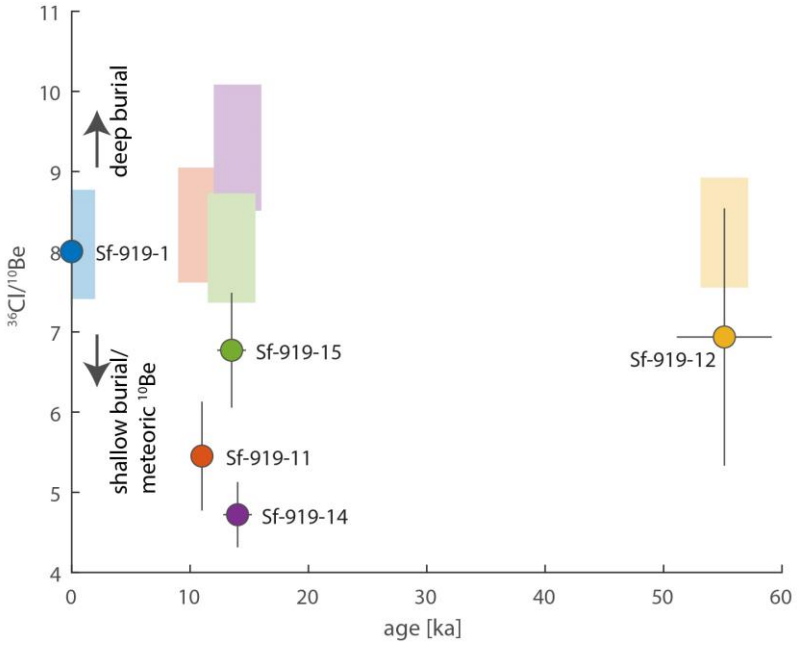

Fig. 10. ^{36}Cl-^{10}Be nuclide ratios of Sfakia fan samples. The shaded boxes indicate the theoretical range of nuclide ratios for erosion rates between 50 and 500 mm/ka. Deep (> 3m) burial within an alluvial fan would shift the ratios to greater values. The expected nuclide ratios vary between samples because the ^{36}Cl production depends on the sample chemistry.

5 Discussion

We investigated the aggradation and incision timing and past variations in denudation rates of two Mediterranean fan systems during the last glacial-interglacial climate cycle. Below, we first discuss the controls on aggradation and incision in our alluvial systems before discussing our paleo-denudation rates. Subsequently, we examine regional changes in climate, sea level, and vegetation throughout the same period and discuss the dominant factors driving changes within these alluvial systems.

5.1 Timing of aggradation and incision

Our geochronologic data show that fan aggradation at the Elafonisi fan sequence occurred during MIS 5b/a (Qt2), MIS 4 to early MIS 3 (Qt3), and MIS 2 (Qt4) (Fig. 4). At the Stomio River mouth, no Qt4 deposit is preserved. Due to its large catchment area, we assume that the Stomio River was able to incise substantially during the low sea level of MIS 2 and likely deposited an MIS 2 fan that now lies offshore. This scenario is supported by the embayment of the coastline directly at the Stomio River mouth (Fig. 2), which suggests river incision during eustatic regression. We did not date Qt1; however, the steep fan-surface gradient suggests deposition during low sea level. Based on its gradient and that the other aggradation events broadly coincide with the end of stadials, we assume deposition of Qt1 during MIS 6. Incision events at the Elafonisi fan broadly coincide with interstadials and interglacials of MIS 1, 3, and 5a.

In contrast to the Elafonisi fan sequence, the Sfakia fan aggraded during most of the past glacial cycle (Pope et al., 2016). However, changes in the aggradation rate may still exist that we can derive from the dated sedimentary cross-sections published by Pope et al. (2008, 2016) (Fig. 11). Combined with accumulation rates from the Chrissoskalitissa fan, dated in this study, aggradation was faster during late MIS 5 and 4 (90 to 60 ka), and especially during MIS 2 (29 to 14 ka) (Fig. 11A). During MIS 1, all fan sections are being incised. However, we note that apparent aggradation rates are typically affected by the timespan of measurement (Sadler, 1981). The timespans represented by our aggradation rates span one order of magnitude and show a moderate decrease with increasing timescale. We thus corrected the aggradation rates for a potential 'Sadler effect' by fitting a power-law through the time-scale – aggradation rate data (Fig. 11B). Subsequently, we used this power-law fit to correct the aggradation rates in Figure 11A. For every aggradation measurement, we calculated an expected aggradation rate based on the power-law fit and subtracted the expected aggradation rate from the measured one (Fig. 11C), similar to the approach of Kemp et al. (2020). These timescale-corrected relative aggradation rates show fast aggradation during MIS 4 and 2 and low rates during early MIS 5 and MIS 3.

We thus conclude that at both study sites, aggradation increased during or towards the end of stadials (MIS 2, 4, 6), and incision or a reduction in aggradation rate occurred during interstadials and interglacials (MIS 1, 3, 5). Additionally, we compiled all geochronologic ages from Pleistocene alluvial fans and river terraces on Crete (n = 49, Fig. 12A). The summed probability density distribution indicates two distinct peaks of aggradation ages, which correspond to MIS 2 and 4 (Fig. 12A) and aligns well with the timing of increased aggradation at the study sites.

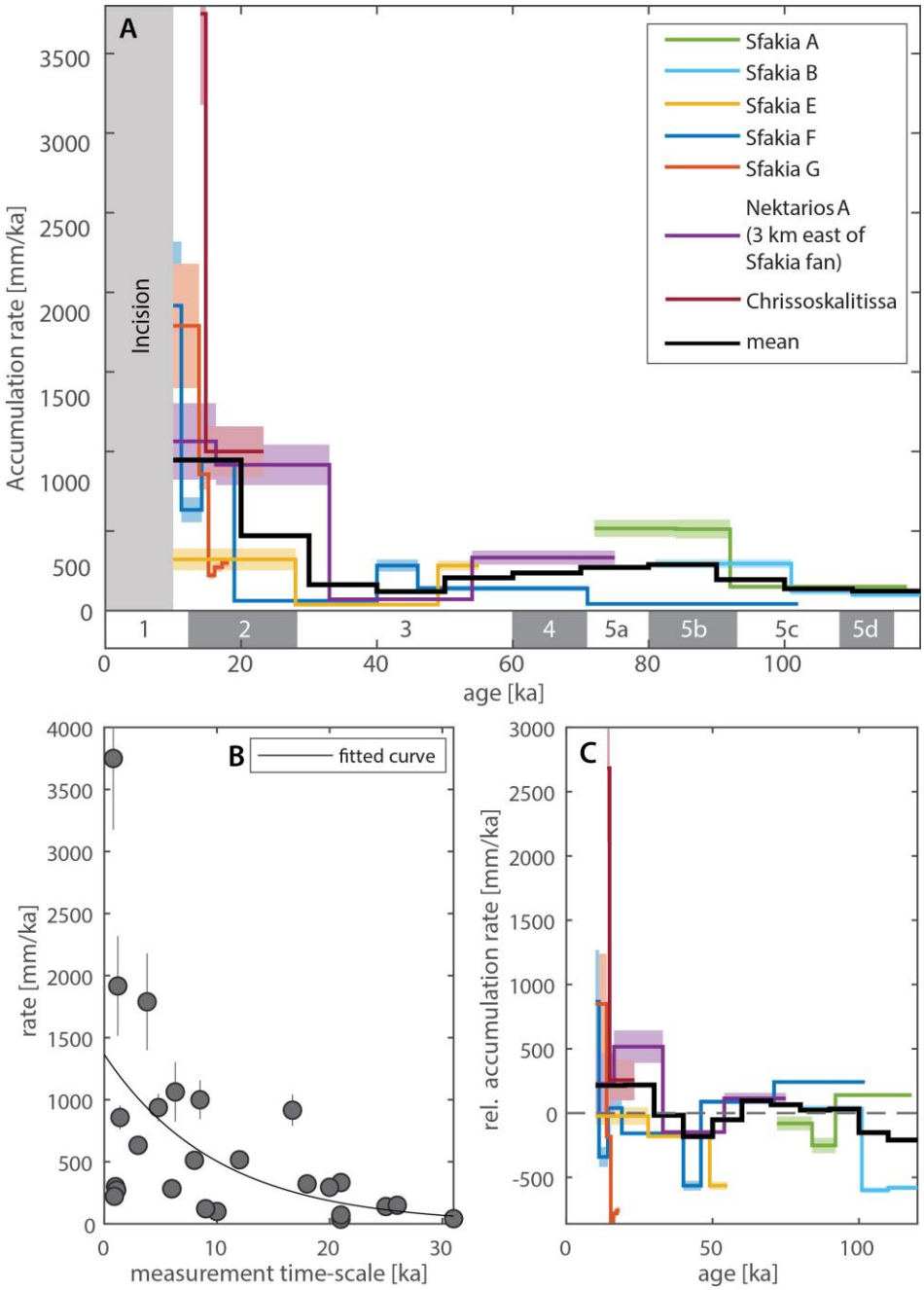

Fig. 11. Accumulation rates of stratigraphic sections published in Pope et al. (2008, 2016) from the Sfakia fans combined with accumulation rates from the Chrissoskalitissa fan. (A) Accumulation rates through time for the different sections. The black line represents the mean of 10 ka bins. (B) Relationship between measurement interval and accumulation rate with a power-law fit. (C) Relative accumulation rates corrected for timescale bias with the power-law fit from (B).

5.2 Paleo-denudation rates

Our paleo-denudation rates are slightly elevated compared to modern denudation rates, although most differences are within the margin of error (Fig. 9). The elevated uncertainty of the reported paleo-denudation rates is partly due to the uncertainty in post-burial nuclide accumulation. However, the largest uncertainties arise from the high [Cl] content of the three samples at Chrissoskalitissa, where large uncertainty on thermal and epithermal neutron production rates complicate the interpretation of changes in denudation rate. In most other samples, the post-burial production component is minor, and even the two depositional scenarios we examined for several samples show < 10% difference in paleo-denudation rates. Therefore, we assume our paleo-denudation rate estimates to be robust.

At the Elafonisi fan system, paleo-denudation rates along the Stomio River are within error of the modern rates measured. The denudation rates in the small Livadia and Chrissoskalitissa fan catchments (~1.5 km² drainage area each) are greater by a factor of 3-9 compared to the Stomio River (35 km²). The Chrissoskalitissa catchment is steeper (32°) than the Livadia (25°) and Stomio (26°) catchments and could explain why this location yields the fastest reported denudation rate so far reported for Crete (Ott et al., 2019a). However, both small catchments yield fast denudation rates, suggesting that the catchment area plays a role in the measured concentrations. In particular, the low paleo-denudation rates at Chrissoskalitissa could be explained by stochastic, low-concentration-sediment input from mass-wasting (Niemi et al., 2005). The Chrissoskalitissa catchment contains significant amounts of gypsum bedrock, which could promote slope failures. Aggradation due to landsliding has been shown to occur in a similar carbonate catchment on Crete (Bruni et al., 2021). However, CRN denudation rates measured elsewhere have been demonstrated to be accurate and consistent despite significant landsliding within catchments (Roda-Boluda et al., 2019), suggesting that mass wasting may not necessarily bias denudation-rate measurements. Alternatively, the shorter catchment length-scale combined with fast denudation rates at Chrissoskalitissa could promote a more rapid response of this catchment to changes in climate compared to larger catchments (Castelltort and Van Den Driessche, 2003; Tofelde et al., 2017; Wickert and Schildgen, 2019). If correct, prolonged sediment mixing and longer sediment transport times in the Stomio River and Sfakia catchment might have damped any climate-driven changes in denudation rate during sediment transport from source to sink. However, the integration times of our paleo-denudation rates are short (<5 ka, Fig. 12C), and sediment storage within the catchments is minor; therefore, it remains unclear whether sediment mixing and storage might have obscured a climate signal.

Our (paleo-)denudation rates are lower than Late Pleistocene coastal uplift rates along Crete's south and west coast (Fig. 5; Ott et al., 2019b). This discrepancy suggests that western Crete experienced net surface uplift during the Late Pleistocene, the rate of which we can crudely estimate by subtracting average denudation from coastal uplift rates. At the Sfakia fan, an average denudation rate of ~ 0.3 mm/a and the average coastal uplift rate at the Levka Ori of 0.8 mm/a (Ott et al., 2019b) suggest 0.5 mm/ka of Levka Ori surface uplift. At Elafonisi, an average denudation rate of ~0.5 mm/a, and ~ 1.3 mm/a coastal uplift rate (Fig. 5) result in a surface uplift rate of about

0.8 mm/a. Higher surface uplift rates in western Crete are consistent with a proposed Late Pleistocene acceleration in uplift inferred along the west coast (Ott et al., 2019b). If these surface uplift rates were constant through time, the 2.5 km elevation of the Levka Ori could have been built within the past 5 Ma, consistent with the island-wide uplift and emergence recorded at the Miocene-Pliocene boundary (van Hinsbergen and Meulenkamp, 2006).

5.3 Linking aggradation, incision and denudation to base-level, climate, and vegetation

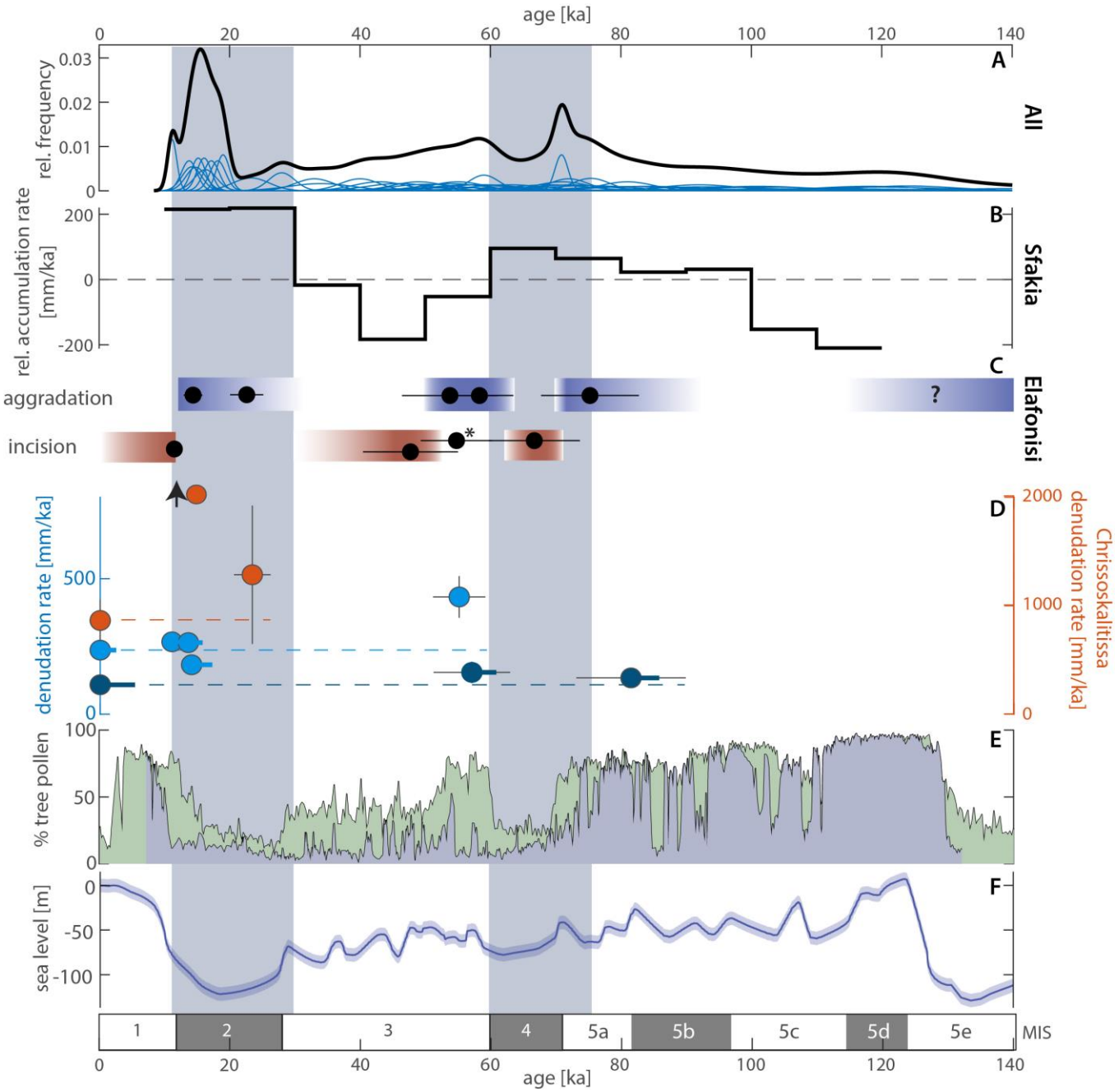

Fig. 12. Summary of aggradation and paleo-denudation data. (A) Individual (blue) and summed probability density functions of compiled geochronologic ages from alluvial fans on Crete (this

study, Gallen et al. 2014, Holcomb et al., 2021, Pope et al. 2008, Pope et al., 2016). (B) Mean relative sediment accumulation rate from Fig. 11C. (C) Aggradation and incision constraints from Elafonisi. (D) Paleo-denudation rates from this study. Denudation rates from the Chrissoskalitissa (orange) are scaled to the right y-axis for visibility. Rates from the Sfakia fan (light blue) and Stomio River (dark blue) are scaled to the left axis. Thick lines behind the dots indicate the approximate integration time of the cosmogenic nuclide sample. Dashed lines correspond to the modern reference values. (E) Percentage of total tree pollen from Tenaghi-Philippon (blue) in the northern Aegean (Wulf et al., 2018) and Ioannina (green) in northwest Greece (Roucoux et al., 2011). We calculated our age model for the Ioannina data based on linear interpolation between dated layers. Hence, the Ioannina pollen record's age uncertainty is greater than Tenaghi-Philippon. (F) Sea-level curve by Lambeck & Chappell (2001).

Periods of pronounced aggradation align with stadials during the last glacial cycle (MIS 2, 4, and 5b) and, therefore, sea-level lowstands. Low sea level during these periods should favour incision in response to a base-level fall and seaward shift of alluvial depocentres. The brief period of incision observed at both study sites at the MIS 5a/4 transition might be an example of such base-level controlled entrenchment. However, incision occurring during sea-level high stands (MIS 1 and 3) suggests that eustasy is only a second-order control on the alluviation dynamics in coastal Crete.

Changes in tectonically-induced base-level fall could also trigger incision. However, the uplift rates derived from paleoshorelines suggest rather constant uplift rates during the Late Pleistocene (Fig. 5), which agrees with the findings of Ott et al. (2019b). Moreover, given that high-amplitude eustatic sea-level variations only had a limited influence on aggradation, it is unlikely that variations in tectonics rates controlled the aggradation behaviour during the Late Pleistocene.

Climate archives from the Eastern Mediterranean show substantial changes in temperature, precipitation, and vegetation throughout the Late Pleistocene: dry and cold conditions during stadials contrast with warm and wet conditions during interstadials and interglacials (Langgut et al., 2011; Wulf et al., 2018). We hypothesize that such variations in climate are the main control on the aggradation and incision behaviour of the studied fans and dominate over the influence of base-level variations.

Aggradation during stadials and incision during interstadials has been observed in other Mediterranean regions (Macklin et al., 2002; Pope and Wilkinson, 2005; Wegmann and Pazzaglia, 2009; Zembo et al., 2009). For instance, Wegmann and Pazzaglia (2009) found that in the Northern Apennines, depending on the hillslope-derived sediment supply, river aggradation or strath terrace formation occurred during stadials with subsequent incision during the transition to interstadials. A compilation of aggradation periods in the Mediterranean by Macklin et al. (2002) documents major aggradation during MIS 6, the MIS 5b/a transition, MIS 4, MIS 2, and universal incision during MIS 1 at all studied sites. These aggradation periods align with the aggradation at the Elafonsi fan system and periods of increased aggradation at the Sfakia fan. About half of the sites

in the Macklin et al. (2002) compilation lie inland. Therefore, the temporal correlation of aggradation and incision in the Eastern Mediterranean is additional evidence that both are mostly governed by climate-related changes in sediment transport, with only second-order controls by tectonics and sea level.

The aggradation behaviour of rivers is a function of sediment supply and transport capacity. Our paleo-denudation rates show that hillslope denudation remained fairly constant throughout the glacial cycle, suggesting no major changes in hillslope denudation during the variations in aggradation and incision. This observation is in agreement with findings from the Northern Apennines, Central Europe, and the Himalaya, where Pleistocene denudation rates remain relatively stable (Schaller et al., 2002; Cyr and Granger, 2008; Kapannusch et al., 2020), despite shifts in river aggradation and incision (Wegmann and Pazzaglia, 2009). However, the fluctuations in precipitation observed by paleoclimate studies in Greece suggest major variations in stream transport capacity during the same time. We thus hypothesize that increased transport capacity due to wet conditions during interstadials and interglacials is probably the main driver of stream incision, whereas reduced transport capacity during stadials led to aggradation. This interpretation suggests that streams in western Crete are transport limited and sensitive to hydroclimate fluctuations.

Changes in climate also led to large fluctuations in vegetation, which may impact sediment supply. Pollen records from northern Greece (Fig. 12E) and Israel show a dominance of forest during interstadials and interglacials and a switch to steppe conditions during stadials (Margari et al., 2009; Roucoux et al., 2011; Langgut et al., 2011; Wulf et al., 2018). Vegetation changes could have modulated the sediment supply to the channel by stabilizing hillslope material (Amundson et al., 2015; Acosta et al., 2015). Therefore, shifts from forest to steppe conditions during stadials may have released pulses of hillslope sediment, leading to aggradation, similar to what can be observed in numerical simulations by Tucker and Slingerland (Tucker and Slingerland, 1997). Faster hillslope transport due to less vegetation would decrease the measured cosmogenic nuclide concentrations (Anderson, 2015). However, this effect may be buffered by (1) the initial release of higher-concentration material that was stabilized, (2) sediment mixing within the catchment, which may dilute the input of low-concentration material from the hillslopes, and (3) the sluggish decrease in CRN concentration due to the integration time of CRNs. Our more variable paleo-denudation rates from the small Chrissoskalitisssa fan could indicate that small catchments with high denudation rates may be capable of registering a short-lived increase in denudation. In the larger Stomio River and Sfakia catchments, sediment storage is limited and integration times of cosmogenic nuclides are short (Fig. 12D). Yet, the addition of various buffering effects may be sufficient to damp a signal in cosmogenic nuclide-derived denudation rates to within uncertainty of modern rates, as observed in this study. Hence, it is likely that the large shifts in vegetation contributed to aggradation and incision by releasing and withholding hillslope sediment, respectively, however the uncertainties and limited number of our paleo-denudation rates do not allow us to infer if changes in hillslope denudation played a secondary role in the aggradation behaviour of streams and alluvial fans.

Relatively steady hillslope denudation during aggradation-incision events has also been observed in the Himalaya (Scherler et al., 2015; Kapannusch et al., 2020). A numerical model of 1-D alluvial river evolution by Simpson and Castelltort (2012) showed that variations in water flux get amplified and transmitted downstream, leading to periods of pronounced aggradation and incision. In contrast, fluctuations in sediment flux get damped on their way from source to sink. Our observations agree well with these findings. Observed variations in sediment flux on Crete were minor and, if present, appear to have been damped over a length-scale of a few kilometres. However, variations in hydroclimate left a strong imprint on the studied coastal alluvial systems, even outcompeting high-amplitude variations in sea level. The consistency between our data, theoretical expectations, and a few other studies suggest that alluvial sequences may rather record variations in hydroclimate than sediment supply in many environments.

6 Summary and Conclusions

We mapped and dated Quaternary alluvial deposits at the Elafonisi and Sfakia fans, Crete, Greece, to determine the timing of aggradation and incision. We combined these data with paleo-denudation rate measurements estimated using concentrations of cosmogenic ^{10}Be and ^{36}Cl to elucidate how climate variations during the last glacial cycle affected sediment production, transport, and deposition.

We identified four Quaternary alluvial units at the Elafonisi fan complex, with geochronologic ages suggesting deposition during MIS 2, 4, 5a/b, and an inferred age of MIS 6. Similarly, aggradation rates at the Sfakia fan suggest the fastest deposition during MIS 2 and 4, with a brief period of minor incision at the MIS 5a/4 boundary and major incision during MIS 1. These periods of aggradation coincide with dry periods and steppe vegetation. We primarily attribute temporal changes in aggradation to decreased stream transport capacity, potentially supported by an increase in hillslope sediment release due to a decline in vegetation cover. Major incision during MIS 1 is likely a response to increased rainfall and stream transport capacity alongside denser vegetation stabilizing hillslope material. An early period of incision at the MIS 5a–4 transition likely occurred in response to rapid sea-level fall, suggesting that base level-driven incision events are superposed onto the climatically-driven sequence of aggradation and incision.

Despite large variations in climate, denudation rates remained relatively constant in western Crete during the Late Pleistocene, except for one small catchment with elevated rates during MIS 2. Hence, we find that streams in western Crete show transport-limited behaviour, where variations in hydroclimate primarily modulate aggradation and incision while denudation rates remain relatively constant. In accordance with numerical models, we speculate that sediment-flux variations are only recorded in small and rapidly eroding basins, while changes in water flux dominate the alluvial record.

Acknowledgments

We thank Negar Haghipour, ETH Zurich for assistance during ^{10}Be sample preparation, and ^{14}C measurements. Richard F. Ott is funded by the Swiss National Science Foundation grant number

P2EZP2_191866. We thank Hellenic Cadastre SA for DEM data. Sincere thanks to Christina Tsimi (NOA) for customizing the 5m digital elevation models for the research area. We thank Emma Lodes for designing the graphical abstract.

References

Acosta, V.T., Schildgen, T.F., Clarke, B.A., Scherler, D., Bookhagen, B., Wittmann, H., Von Blanckenburg, F., and Strecker, M.R., 2015, Effect of vegetation cover on millennial-scale landscape denudation rates in East Africa: Lithosphere, v. 7, p. 408–420, doi:10.1130/L402.1.

Adamiec, G., and Aitken, M.J., 1998, Dose-rate conversion factors: update: Ancient tL, v. 16, p. 37–50.

Aitken, M.J. (Martin J., 1998, An introduction to optical dating : the dating of Quaternary sediments by the use of photon-stimulated luminescence: , p. 267.

Amundson, R., Heimsath, A., Owen, J., Yoo, K., and Dietrich, W.E., 2015, Hillslope soils and vegetation: Geomorphology, v. 234, p. 122–132, doi:10.1016/J.GEOMORPH.2014.12.031.

Anderson, R.S., 2015, Particle trajectories on hillslopes: Implications for particle age and 10Be structure: Journal of Geophysical Research F: Earth Surface, v. 119, p. 1–20, doi:10.1002/2013JF002950.Received.

Angelier, J., 1979, Recent quaternary tectonics in the hellenic arc; examples of geological observations on land; recent crustal movements: Tectonophysics, v. 52, p. 267–275.

Beck, H.E., Zimmermann, N.E., McVicar, T.R., Vergopolan, N., Berg, A., and Wood, E.F., 2018, Present and future Köppen-Geiger climate classification maps at 1-km resolution: Scientific Data 2018 5:1, v. 5, p. 1–12, doi:10.1038/sdata.2018.214.

Berger, A.L. et al., 2008, Quaternary tectonic response to intensified glacial erosion in an orogenic wedge: Nature Geoscience 2008 1:11, v. 1, p. 793–799, doi:10.1038/ngeo334.

Bierman, P.R., Caffee, M.W., Davis, P.T., Marsella, K., Pavich, M., Colgan, P., Mickelson, D., and Larsen, J., 2002, Rates and timing of Earth surface processes from In Situ-produced cosmogenic Be-10, *in* Beryllium: Mineralogy, Petrology, and Geochemistry, De Gruyter Mouton, v. 50, p. 147–205, doi:10.2138/rmg.2002.50.4.

Bruni, E.T., Ott, R.F., Picotti, V., Haghipour, N., Wegmann, K.W., and Gallen, S.F., 2021, Stochastic alluvial fan and terrace formation triggered by a high-magnitude Holocene landslide in the Klados Gorge, Crete: Earth Surface Dynamics, v. 9, p. 771–793, doi:10.5194/esurf-9-771-2021.

Bull, W.B., 1991, Geomorphic responses to climatic change: United States, New York, NY (United States); Oxford University Press, https://www.osti.gov/biblio/5603696.

Castelltort, S., and Van Den Driessche, J., 2003, How plausible are high-frequency sediment supply-driven cycles in the stratigraphic record? Sedimentary Geology, v. 157, p. 3–13,

doi:10.1016/S0037-0738(03)00066-6.

Cheddadi, R., and Rossignol-Strick, M., 1995, Eastern Mediterranean Quaternary paleoclimates from pollen and isotope records of marine cores in the Nile Cone Area: Paleoceanography, v. 10, p. 291–300, doi:10.1029/94PA02672.

Christl, M., Vockenhuber, C., Kubik, P.W., Wacker, L., Lachner, J., Alfimov, V., and Synal, H.-A., 2013, The ETH Zurich AMS facilities: Nuclear Instruments and Methods in Physics Research Section B: Beam Interactions with Materials and Atoms, v. 294, p. 29–38, doi:10.1016/j.nimb.2012.03.004.

Creutzberg, N., Drooger, C.W., Meulenkamp, J.E., Papastamatiou, J., Sannemann, W., Seidel, E., and Tatares, A., 1977, General Geological Map of the Island of Crete, 1: 200,000: Institute of Geology and Mineral Exploration, Athens,.

Cyr, A.J., and Granger, D.E., 2008, Dynamic equilibrium among erosion, river incision, and coastal uplift in the northern and central Apennines, Italy: Geology, v. 36, p. 103–106, doi:10.1130/G24003A.1.

D'Arcy, M., Roda-Boluda, D.C., and Whittaker, A.C., 2017a, Glacial-interglacial climate changes recorded by debris flow fan deposits, Owens Valley, California: Quaternary Science Reviews, v. 169, p. 288–311, doi:10.1016/J.QUASCIREV.2017.06.002.

D'Arcy, M., Whittaker, A.C., and Roda-Boluda, D.C., 2017b, Measuring alluvial fan sensitivity to past climate changes using a self-similarity approach to grain-size fining, Death Valley, California: Sedimentology, v. 64, p. 388–424, doi:10.1111/SED.12308.

Dewald, A. et al., 2013, CologneAMS, a dedicated center for accelerator mass spectrometry in Germany, *in* Nuclear Instruments and Methods in Physics Research, Section B: Beam Interactions with Materials and Atoms, North-Holland, v. 294, p. 18–23, doi:10.1016/j.nimb.2012.04.030.

Fassoulas, C., Kilias, A., and Mountrakis, D., 1994, Postnappe stacking extension and exhumation of high-pressure/low-temperature rocks in the island of Crete, Greece: Tectonics, v. 13, p. 127–138, doi:10.1029/93TC01955.

Ferrier, G., and Pope, R.J.J., 2012, Quantitative mapping of alluvial fan evolution using ground-based reflectance spectroscopy: Geomorphology, v. 175–176, p. 14–24, doi:10.1016/J.GEOMORPH.2012.06.013.

Galbraith, R.F., and Roberts, R.G., 2012, Statistical aspects of equivalent dose and error calculation and display in OSL dating: An overview and some recommendations: Quaternary Geochronology, v. 11, p. 1–27, doi:10.1016/J.QUAGEO.2012.04.020.

Gallen, S.F., Wegmann, K.W., Bohnenstiehl, D.R., Pazzaglia, F.J., Brandon, M.T., and Fassoulas, C., 2014, Active simultaneous uplift and margin-normal extension in a forearc high, Crete, Greece: Earth and Planetary Science Letters, v. 398, p. 11–24, doi:10.1016/j.epsl.2014.04.038.

Geyh, M.A., and Eitel, B., 1997, Radiometric Dating of Young and Old Calcrete: Radiocarbon, v. 40, p. 795–802, doi:10.1017/S0033822200018749.

Giresse, P., and Martzluff, M., 2015, AMS radiocarbon dating of carbonate cements in late Pleistocene alluvial conglomerates, Verdouble River. Palaeoenvironmental implications concerning the Palaeolithic site of Tautavel (Pyrénées-Orientales): Geomorphologie, v. 21, p. 115–130, doi:10.4000/GEOMORPHOLOGIE.10956.

Guérin, G., Mercier, N., and Adamiec, G., 2011, Dose-rate conversion factors: update: Ancient Tl, v. 29, p. 5–8.

Hales, T.C., and Roering, J.J., 2007, Climatic controls on frost cracking and implications for the evolution of bedrock landscapes: Journal of Geophysical Research: Earth Surface, v. 112, p. 2033, doi:10.1029/2006JF000616.

Harvey, A.M., Silva, P.G., Mather, A.E., Goy, J.L., Stokes, M., and Zazo, C., 1999, The impact of Quaternary sea-level and climatic change on coastal alluvial fans in the Cabo de Gata ranges, southeast Spain: Geomorphology, v. 28, p. 1–22, doi:10.1016/S0169-555X(98)00100-7.

Herman, F., Seward, D., Valla, P.G., Carter, A., Kohn, B., Willett, S.D., and Ehlers, T.A., 2013, Worldwide acceleration of mountain erosion under a cooling climate: Nature, v. 504, p. 423–426, doi:10.1038/nature12877.

van Hinsbergen, D.J., and Meulenkamp, J.E., 2006, Neogene supradetachment basin development on Crete (Greece) during exhumation of the South Aegean core complex: Basin Research, v. 18, p. 103–124, doi:10.1111/j.1365-2117.2005.00282.x.

Holcomb, J.A., Wegmann, K.W., and Runnels, C.N., 2021, Late Quaternary coastal stratigraphy at Mochlos Bay, northeast Crete, Greece: Implications for palaeolithic archaeological site preservation and hominin dispersals: Geological Society of America Abstracts with Programs, v. 53, doi:10.1130/abs/2021AM-369290.

Hughes, P.D., and Woodward, J.C., 2017, Quaternary glaciation in the Mediterranean mountains: a new synthesis: Geological Society, London, Special Publications, v. 433, p. 1–23, doi:10.1144/SP433.14.

Ivy-Ochs, S., Synal, H.-A., Roth, C., and Schaller, M., 2004, Initial results from isotope dilution for Cl and 36Cl measurements at the PSI/ETH Zurich AMS facility: Nuclear Instruments and Methods in Physics Research Section B: Beam Interactions with Materials and Atoms, v. 223–224, p. 623–627, doi:10.1016/j.nimb.2004.04.115.

Jolivet, L., and Brun, J.-P., 2010, Cenozoic geodynamic evolution of the Aegean: International Journal of Earth Sciences, v. 99, p. 109–138, doi:10.1007/s00531-008-0366-4.

Kapannusch, R., Scherler, D., King, G., and Wittmann, H., 2020, Glacial influence on late Pleistocene 10Be-derived paleo-erosion rates in the north-western Himalaya, India: Earth and Planetary Science Letters, v. 547, p. 116441, doi:10.1016/j.epsl.2020.116441.

Kemp, D.B., Sadler, P.M., and Vanacker, V., 2020, The human impact on North American erosion, sediment transfer, and storage in a geologic context: Nature Communications 2020 11:1, v. 11, p. 1–9, doi:10.1038/s41467-020-19744-3.

Lajoie, K.R., 1986, Coastal tectonics, *in* Wallace, R. ed., Active Tectonics, Washington, D.C., National Academy Press, Studies in Geophysics Series, Geophysics Research Forum, p. 95–124.

Lambeck, K., and Chappell, J., 2001, Sea Level Change Through the Last Glacial Cycle: Science, v. 292, p. 679–686, doi:10.1126/science.1059549.

Langgut, D., Almogi-Labin, A., Bar-Matthews, M., and Weinstein-Evron, M., 2011, Vegetation and climate changes in the South Eastern Mediterranean during the Last Glacial-Interglacial cycle (86 ka): new marine pollen record: Quaternary Science Reviews, v. 30, p. 3960–3972, doi:10.1016/J.QUASCIREV.2011.10.016.

Lenard, S.J.P., Lavé, J., France-Lanord, C., Aumaître, G., Bourlès, D.L., and Keddadouche, K., 2020, Steady erosion rates in the Himalayas through late Cenozoic climatic changes: Nature Geoscience, v. 13, doi:10.1038/s41561-020-0585-2.

Macklin, M.G., Fuller, I.C., Lewin, J., Maas, G.S., Passmore, D.G., Rose, J., Woodward, J.C., Black, S., Hamlin, R.H.B., and Rowan, J.S., 2002, Correlation of fluvial sequences in the Mediterranean basin over the last 200ka and their relationship to climate change: Quaternary Science Reviews, v. 21, p. 1633–1641, doi:10.1016/S0277-3791(01)00147-0.

Margari, V., Gibbard, P.L., Bryant, C.L., and Tzedakis, P.C., 2009, Character of vegetational and environmental changes in southern Europe during the last glacial period; evidence from Lesvos Island, Greece: Quaternary Science Reviews, v. 28, p. 1317–1339, doi:10.1016/J.QUASCIREV.2009.01.008.

Mariotti, A., Blard, P.H., Charreau, J., Toucanne, S., Jorry, S.J., Molliex, S., Bourlès, D.L., Aumaître, G., and Keddadouche, K., 2021, Nonlinear forcing of climate on mountain denudation during glaciations: Nature Geoscience, v. 14, p. 16–22, doi:10.1038/s41561-020-00672-2.

Marrero, S.M., Phillips, F.M., Borchers, B., Lifton, N., Aumer, R., and Balco, G., 2016a, Cosmogenic nuclide systematics and the CRONUScalc program: Quaternary Geochronology, v. 31, p. 160–187, doi:10.1016/j.quageo.2015.09.005.

Marrero, S.M., Phillips, F.M., Caffee, M.W., and Gosse, J.C., 2016b, CRONUS-Earth cosmogenic 36 Cl calibration: Quaternary Geochronology, v. 31, p. 199–219, doi:10.1016/j.quageo.2015.10.002.

Marshall, J.A., Roering, J.J., Bartlein, P.J., Gavin, D.G., Granger, D.E., Rempel, A.W., Praskievicz, S.J., and Hales, T.C., 2015, Earth Sciences: Frost for the Trees: Did climate increase erosion in unglaciated landscapes during the late Pleistocene? Science Advances, v. 1, p. e1500715, doi:10.1126/sciadv.1500715.

Marshall, J.A., Roering, J.J., Rempel, A.W., Shafer, S.L., and Bartlein, P.J., 2021, Extensive Frost Weathering Across Unglaciated North America During the Last Glacial Maximum: Geophysical Research Letters, v. 48, p. e2020GL090305, doi:10.1029/2020GL090305.

Mason, C.C., and Romans, B.W., 2018, Climate-driven unsteady denudation and sediment flux in a high-relief unglaciated catchment–fan using 26Al and 10Be: Panamint Valley, California: Earth and Planetary Science Letters, v. 492, p. 130–143, doi:10.1016/j.epsl.2018.03.056.

Mountrakis, D., Kilias, A., Pavlaki, A., Fassoulas, C., Thomaidou, E., Papazachos, C., Papaioannou, C., Roumelioti, Z., Benetatos, C., and Vamvarakis, D., 2012, Neotectonic study of the western Crete. Seismic risk evaluation of the active faults: J. Virtual Explorer, v. 42.

Murray, A.S., and Wintle, A.G., 2000, Luminescence dating of quartz using an improved single-aliquot regenerative-dose protocol: Radiation Measurements, v. 32, p. 57–73, doi:10.1016/S1350-4487(99)00253-X.

Nemec, W., and Postma, G., 1993, Quaternary Alluvial Fans in Southwestern Crete: Sedimentation Processes and Geomorphic Evolution: Alluvial Sedimentation, p. 235–276, doi:10.1002/9781444303995.CH18.

Niemi, N.A., Oskin, M., Burbank, D.W., Heimsath, A.M., and Gabet, E.J., 2005, Effects of bedrock landslides on cosmogenically determined erosion rates: Earth and Planetary Science Letters, v. 237, p. 480–498, doi:10.1016/j.epsl.2005.07.009.

Nishiizumi, K., Winterer, E., Kohl, C., Klein, J., Middleton, R., Lal, D., Arnold, J.R., and Jolla, L., 1989, Cosmic ray production rates of 10Be and 26Al in quartz from glacially polished rocks: Journal of Geophysical Research: Solid Earth, v. 94, p. 17907–17915, doi:10.1029/JB094IB12P17907.

Ott, R.F., 2020, How Lithology Impacts Global Topography, Vegetation, and Animal Biodiversity: A Global-Scale Analysis of Mountainous Regions: Geophysical Research Letters, v. 47, doi:10.1029/2020GL088649.

Ott, R.F., 2022, POST PRO - POSTburial PROduction for cosmogenic nuclide samples: GFZ Data Services, doi:10.5880/GFZ.3.3.2022.002.

Ott, R.F., Gallen, S.F., Caves Rugenstein, J.K., Ivy-Ochs, S., Helman, D., Fassoulas, C., Vockenhuber, C., Christl, M., and Willett, S.D., 2019a, Chemical Versus Mechanical Denudation in Meta-Clastic and Carbonate Bedrock Catchments on Crete, Greece, and Mechanisms for Steep and High Carbonate Topography: Journal of Geophysical Research: Earth Surface, v. 124, p. 2943–2961, doi:10.1029/2019JF005142.

Ott, R.F., Gallen, S.F., Wegmann, K.W., Biswas, R.H., Herman, F., and Willett, S.D., 2019b, Pleistocene terrace formation, Quaternary rock uplift rates and geodynamics of the Hellenic Subduction Zone revealed from dating of paleoshorelines on Crete, Greece.: Earth and Planetary Science Letters, v. 525, p. 115757, doi:10.1016/j.epsl.2019.115757.

Ott, R.F., Wegmann, K.W., Gallen, S.F., Pazzaglia, F.J., Brandon, M.T., Ueda, K., and Fassoulas,

C., 2021, Reassessing Eastern Mediterranean Tectonics and Earthquake Hazard From the 365 CE Earthquake: AGU Advances, v. 2, p. e2020AV000315, doi:10.1029/2020AV000315.

Peizhen, Z., Molnar, P., and Downs, W.R., 2001, Increased sedimentation rates and grain sizes 2–4 Myr ago due to the influence of climate change on erosion rates: Nature 2001 410:6831, v. 410, p. 891–897, doi:10.1038/35073504.

Phillips, F.M. et al., 2016, The CRONUS-Earth Project: A synthesis: Quaternary Geochronology, v. 31, p. 119–154, doi:10.1016/j.quageo.2015.09.006.

Pope, R.J.J., Candy, I., and Skourtsos, E., 2016, A chronology of alluvial fan response to Late Quaternary sea level and climate change, Crete: Quaternary Research, doi:10.1016/j.yqres.2016.06.003.

Pope, R.J.J., and Wilkinson, K.N., 2005, Reconciling the roles of climate and tectonics in Late Quaternary fan development on the Spartan piedmont, Greece: Geological Society Special Publication, v. 251, p. 133–152, doi:10.1144/GSL.SP.2005.251.01.10.

Pope, R., Wilkinson, K., Skourtsos, E., Triantaphyllou, M., and Ferrier, G., 2008, Clarifying stages of alluvial fan evolution along the Sfakian piedmont, southern Crete: New evidence from analysis of post-incisive soils and OSL dating: Geomorphology, v. 94, p. 206–225, doi:10.1016/j.geomorph.2007.05.007.

Prager, C., Ivy-Ochs, S., Ostermann, M., Synal, H.-A., and Patzelt, G., 2009, Geology and radiometric 14C-, 36Cl- and Th-/U-dating of the Fernpass rockslide (Tyrol, Austria): Geomorphology, v. 103, p. 93–103, doi:10.1016/j.geomorph.2007.10.018.

Prescott, J.R., and Hutton, J.T., 1994, Cosmic ray contributions to dose rates for luminescence and ESR dating: Large depths and long-term time variations: Radiation Measurements, v. 23, p. 497–500, doi:10.1016/1350-4487(94)90086-8.

Reilinger, R. et al., 2006, GPS constraints on continental deformation in the Africa-Arabia-Eurasia continental collision zone and implications for the dynamics of plate interactions: Journal of Geophysical Research, v. 111, p. 26, doi:10.1029/2005JB004051.

Reilinger, R., McClusky, S., Paradissis, D., Ergintav, S., and Vernant, P., 2010, Geodetic constraints on the tectonic evolution of the Aegean region and strain accumulation along the Hellenic subduction zone: Tectonophysics, v. 488, p. 22–30, doi:10.1016/j.tecto.2009.05.027.

Reimer, P.J. et al., 2020, The IntCal20 Northern Hemisphere Radiocarbon Age Calibration Curve (0–55 cal kBP): Radiocarbon, v. 62, p. 725–757, doi:10.1017/RDC.2020.41.

Richardson, P.W., Perron, J.T., and Schurr, N.D., 2019, Influences of climate and life on hillslope sediment transport: Geology, v. 47, p. 423–426, doi:10.1130/G45305.1.

Rittenour, T.M., Goble, R.J., and Blum, M.D., 2003, An optical age chronology of Late Pleistocene fluvial deposits in the northern lower Mississippi valley: Quaternary Science Reviews, v. 22,

p. 1105–1110, doi:10.1016/S0277-3791(03)00041-6.

Rittenour, T.M., Goble, R.J., and Blum, M.D., 2005, Development of an OSL chronology for Late Pleistocene channel belts in the lower Mississippi valley, USA: Quaternary Science Reviews, v. 24, p. 2539–2554, doi:10.1016/J.QUASCIREV.2005.03.011.

Robertson, J., Meschis, M., Roberts, G.P., Ganas, A., and Gheorghiu, D.M., 2019, Temporally Constant Quaternary Uplift Rates and Their Relationship With Extensional Upper-Plate Faults in South Crete (Greece), Constrained With 36Cl Cosmogenic Exposure Dating: Tectonics, v. 38, p. 1189–1222, doi:10.1029/2018TC005410.

Roda-Boluda, D.C., D'Arcy, M., Whittaker, A.C., Gheorghiu, D.M., and Rodés, Á., 2019, 10Be erosion rates controlled by transient response to normal faulting through incision and landsliding: Earth and Planetary Science Letters, v. 507, p. 140–153, doi:10.1016/j.epsl.2018.11.032.

Rodés, Á., Pallàs, R., Braucher, R., Moreno, X., Masana, E., and Bourlés, L., 2011, Effect of density uncertainties in cosmogenic 10 Be depth-profiles: Dating a cemented Pleistocene alluvial fan (Carboneras Fault, SE Iberia): Quaternary Geochronology, v. 6, p. 186–194, doi:10.1016/j.quageo.2010.10.004.

Roucoux, K.H., Tzedakis, P.C., Lawson, I.T., and Margari, V., 2011, Vegetation history of the penultimate glacial period (Marine isotope stage 6) at Ioannina, north-west Greece: Journal of Quaternary Science, v. 26, p. 616–626, doi:10.1002/JQS.1483.

Sadler, P.M., 1981, Sediment Accumulation Rates and the Completeness of Stratigraphic Sections: https://doi.org/10.1086/628623, v. 89, p. 569–584, doi:10.1086/628623.

Schaller, M., Blanckenburg, F., Veldkamp, A., Tebbens, L.A., Hovius, N., and Kubik, P.W., 2002, A 30 000 yr record of erosion rates from cosmogenic 10Be in Middle European river terraces: Earth and Planetary Science Letters, v. 204, p. 307–320, doi:10.1016/S0012-821X(02)00951-2.

Scherler, D., Bookhagen, B., Wulf, H., Preusser, F., and Strecker, M.R., 2015, Increased late Pleistocene erosion rates during fluvial aggradation in the Garhwal Himalaya, northern India: Earth and Planetary Science Letters, v. 428, p. 255–266, doi:10.1016/j.epsl.2015.06.034.

Schildgen, T.F., Van Der Beek, P.A., Sinclair, H.D., and Thiede, R.C., 2018, Spatial correlation bias in late-Cenozoic erosion histories derived from thermochronology: Nature, v. 559, p. 89–93, doi:10.1038/s41586-018-0260-6.

Shaw, B., Ambraseys, N.N., England, P.C., Floyd, M.A., Gorman, G.J., Higham, T.F.G., Jackson, J.A., Nocquet, J.M., Pain, C.C., and Piggott, M.D., 2008, Eastern Mediterranean tectonics and tsunami hazard inferred from the AD 365 earthquake: Nature Geoscience, v. 1, p. 268–276, doi:10.1038/ngeo151.

Shuster, D.L., Ehlers, T.A., Rusmore, M.E., and Farley, K.A., 2005, Geology: Rapid glacial erosion at 1.8 Ma revealed by 4He/ 3He thermochronometry: Science, v. 310, p. 1668–1670,

doi:10.1126/science.1118519.

Simpson, G., and Castelltort, S., 2012, Model shows that rivers transmit high-frequency climate cycles to the sedimentary record: Geology, v. 40, p. 1131–1134, doi:10.1130/G33451.1.

Stone, J.O., 2000, Air pressure and cosmogenic isotope production: Journal of Geophysical Research: Solid Earth, v. 105, p. 23753–23759, doi:10.1029/2000JB900181.

Strasser, T.F., Runnels, C., Wegmann, K., Panagopoulou, E., McCoy, F., Digregorio, C., Karkanas, P., and Thompson, N., 2011, Dating Palaeolithic sites in southwestern Crete, Greece: Journal of Quaternary Science, v. 26, p. 553–560, doi:10.1002/jqs.1482.

Stuiver, M., and Polach, H.A., 1977, Discussion Reporting of 14C Data: Radiocarbon, v. 19, p. 355–363, doi:10.1017/S0033822200003672.

Synal, H.-A., Stocker, M., and Suter, M., 2007, MICADAS: A new compact radiocarbon AMS system: Nuclear Instruments and Methods in Physics Research Section B: Beam Interactions with Materials and Atoms, v. 259, p. 7–13, doi:10.1016/j.nimb.2007.01.138.

Tofelde, S., Schildgen, T.F., Savi, S., Pingel, H., Wickert, A.D., Bookhagen, B., Wittmann, H., Alonso, R.N., Cottle, J., and Strecker, M.R., 2017, 100 kyr fluvial cut-and-fill terrace cycles since the Middle Pleistocene in the southern Central Andes, NW Argentina: Earth and Planetary Science Letters, v. 473, p. 141–153, doi:10.1016/J.EPSL.2017.06.001.

Tucker, G.E., and Slingerland, R., 1997, Drainage basin responses to climate change: Water Resources Research, v. 33, p. 2031–2047, doi:10.1029/97WR00409.

Valla, P.G., Van Der Beek, P.A., Shuster, D.L., Braun, J., Herman, F., Tassan-Got, L., and Gautheron, C., 2012, Late Neogene exhumation and relief development of the Aar and Aiguilles Rouges massifs (Swiss Alps) from low-temperature thermochronology modeling and 4He/3He thermochronometry: Journal of Geophysical Research: Earth Surface, v. 117, p. 1004, doi:10.1029/2011JF002043.

Vernon, A.J., van der Beek, P.A., Sinclair, H.D., and Rahn, M.K., 2008, Increase in late Neogene denudation of the European Alps confirmed by analysis of a fission-track thermochronology database: Earth and Planetary Science Letters, v. 270, p. 316–329, doi:10.1016/J.EPSL.2008.03.053.

Vockenhuber, C., Miltenberger, K.-U., and Synal, H.-A., 2019, 36Cl measurements with a gas-filled magnet at 6 MV: Nuclear Instruments and Methods in Physics Research Section B: Beam Interactions with Materials and Atoms, doi:10.1016/j.nimb.2018.12.046.

Waters, J. V., Jones, S.J., and Armstrong, H.A., 2010, Climatic controls on late Pleistocene alluvial fans, Cyprus: Geomorphology, v. 115, p. 228–251, doi:10.1016/J.GEOMORPH.2009.09.002.

Watkins, S.E., Whittaker, A.C., Bell, R.E., McNeill, L.C., Gawthorpe, R.L., Brooke, S.A.S., and Nixon, C.W., 2019, Are landscapes buffered to high-frequency climate change? A

comparison of sediment fluxes and depositional volumes in the Corinth Rift, central Greece, over the past 130 k.y.: GSA Bulletin, v. 131, p. 372–388, doi:10.1130/B31953.1.

Wegmann, K.W., and Pazzaglia, F.J., 2009, Late Quaternary fluvial terraces of the Romagna and Marche Apennines, Italy: Climatic, lithologic, and tectonic controls on terrace genesis in an active orogen: Quaternary Science Reviews, v. 28, p. 137–165, doi:10.1016/j.quascirev.2008.10.006.

Wickert, A.D., and Schildgen, T.F., 2019, Long-profile evolution of transport-limited gravel-bed rivers: Earth Surface Dynamics, v. 7, p. 17–43, doi:10.5194/esurf-7-17-2019.

Willenbring, J.K., and von Blanckenburg, F., 2010, Long-term stability of global erosion rates and weathering during late-Cenozoic cooling: Nature, v. 465, p. 211–214, doi:10.1038/nature09044.

Willenbring, J.K., and Jerolmack, D.J., 2016, The null hypothesis: steady rates of erosion, weathering and sediment accumulation during Late Cenozoic mountain uplift and glaciation.: Terra Nova, v. 28, p. 11–18, doi:10.1111/ter.12185.

Wintle, A.G., and Murray, A.S., 2006, A review of quartz optically stimulated luminescence characteristics and their relevance in single-aliquot regeneration dating protocols: Radiation Measurements, v. 41, p. 369–391, doi:10.1016/J.RADMEAS.2005.11.001.

Wulf, S. et al., 2018, The marine isotope stage 1–5 cryptotephra record of Tenaghi Philippon, Greece: Towards a detailed tephrostratigraphic framework for the Eastern Mediterranean region: Quaternary Science Reviews, v. 186, p. 236–262, doi:10.1016/j.quascirev.2018.03.011.

Zembo, I., Panzeri, L., Galli, A., Bersezio, R., Martini, M., and Sibilia, E., 2009, Quaternary evolution of the intermontane Val d'Agri Basin, Southern Apennines: Quaternary Research, v. 72, p. 431–442, doi:10.1016/J.YQRES.2009.02.009.

Zerathe, S., Braucher, R., Lebourg, T., Bourlès, D., Manetti, M., and Léanni, L., 2013, Dating chert (diagenetic silica) using in-situ produced 10Be: Possible complications revealed through a comparison with 36Cl applied to coexisting limestone: Quaternary Geochronology, v. 17, p. 81–93, doi:10.1016/j.quageo.2013.01.003.